NASA/TP—2000–209892

One-Dimensional Coupled Ecosystem-Carbon Flux Model for the Simulation of Biogeochemical Parameters at Ocean Weather Station P

S. Signorini, C. McClain, J. Christian, and C.S. Wong

National Aeronautics and
Space Administration

Goddard Space Flight Center
Greenbelt, Maryland 20771

June 2000

The NASA STI Program Office … in Profile

Since its founding, NASA has been dedicated to the advancement of aeronautics and space science. The NASA Scientific and Technical Information (STI) Program Office plays a key part in helping NASA maintain this important role.

The NASA STI Program Office is operated by Langley Research Center, the lead center for NASA's scientific and technical information. The NASA STI Program Office provides access to the NASA STI Database, the largest collection of aeronautical and space science STI in the world. The Program Office is also NASA's institutional mechanism for disseminating the results of its research and development activities. These results are published by NASA in the NASA STI Report Series, which includes the following report types:

- TECHNICAL PUBLICATION. Reports of completed research or a major significant phase of research that present the results of NASA programs and include extensive data or theoretical analysis. Includes compilations of significant scientific and technical data and information deemed to be of continuing reference value. NASA's counterpart of peer-reviewed formal professional papers but has less stringent limitations on manuscript length and extent of graphic presentations.
- TECHNICAL MEMORANDUM. Scientific and technical findings that are preliminary or of specialized interest, e.g., quick release reports, working papers, and bibliographies that contain minimal annotation. Does not contain extensive analysis.
- CONTRACTOR REPORT. Scientific and technical findings by NASA-sponsored contractors and grantees.
- CONFERENCE PUBLICATION. Collected papers from scientific and technical conferences, symposia, seminars, or other meetings sponsored or cosponsored by NASA.
- SPECIAL PUBLICATION. Scientific, technical, or historical information from NASA programs, projects, and mission, often concerned with subjects having substantial public interest.
- TECHNICAL TRANSLATION. English-language translations of foreign scientific and technical material pertinent to NASA's mission.

Specialized services that complement the STI Program Office's diverse offerings include creating custom thesauri, building customized databases, organizing and publishing research results . . . even providing videos.

For more information about the NASA STI Program Office, see the following:

- Access the NASA STI Program Home Page at http://www.sti.nasa.gov/STI-homepage.html
- E-mail your question via the Internet to help@sti.nasa.gov
- Fax your question to the NASA Access Help Desk at (301) 621-0134
- Telephone the NASA Access Help Desk at (301) 621-0390
- Write to:
  NASA Access Help Desk
  NASA Center for AeroSpace Information
  7121 Standard Drive
  Hanover, MD 21076-1320

NASA/TP—2000–209892

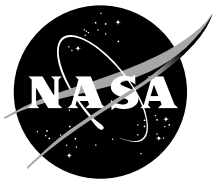

One-Dimensional Coupled Ecosystem-Carbon Flux Model for the Simulation of Biogeochemical Parameters at Ocean Weather Station P

Sergio R. Signorini, SAIC General Sciences Corporation, Beltsville, Maryland
Charles R. McClain, NASA Goddard Space Flight Center, Greenbelt, Maryland
James R. Christian, Universities Space Research Association, NASA GSFC, Greenbelt, Maryland
C.S. Wong, Centre for Ocean Climatic Chemistry, Institute of Ocean Sciences, Sidney, BC, Canada

National Aeronautics and
Space Administration

Goddard Space Flight Center
Greenbelt, Maryland 20771

June 2000

Acknowledgments

We acknowledge the support provided by NASA's Ocean Biogeochemistry Program (NASA RTOP 622-51-30). We are thankful to Dr. Paulette Murphy for enlightening discussions regarding the chemical thermodynamics aspects of this work. We are also thankful to Dr. David Antoine for sharing his carbon chemistry Fortran code with us. Finally, we would like to acknowledge Dr. Ina Tegen for the atmospheric dust model results, Moss Landing Marine Labs for the iron data, and Dr. Ragu Murtuggude for providing the simulated (OGCM) ocean currents.

Available from:

NASA Center for AeroSpace Information
7121 Standard Drive
Hanover, MD 21076-1320
Price Code: A17

National Technical Information Service
5285 Port Royal Road
Springfield, VA 22161
Price Code: A10

PROLOGUE

The global oceans contain approximately 50 times as much CO_2 in dissolved forms as that in the atmosphere, while the land biosphere including the biota and soil carbon contains about 3 times as much carbon (as CO_2) as that in the atmosphere (*Sundquist*, 1985). Thus the spatial and temporal variability of CO_2 fluxes over the ocean are crucial for projecting the future level of atmospheric CO_2.

One of the most important parameters of the oceanic CO_2 system is the partial pressure of dissolved carbon dioxide, pCO_2, in the surface ocean (*Takahashi et al*., 1993; *Wong and Chan*, 1991). The difference between pCO_2 in surface seawater and in the overlying atmosphere defines the source and sink areas of CO_2 over the global oceans. Since the high latitude waters are probably undersaturated with respect to CO_2 in the summer (*Keeling*, 1968), these oceanic areas could play an important role in climate-CO_2 feedback processes by removing large quantities of CO_2 from the atmosphere (*Wong and Chan*, 1991). Temperate and polar oceans of both hemispheres are the major sinks for atmospheric CO_2, whereas the equatorial oceans are the major sources for CO_2 (*Takahashi et al*., 1997). Thus, the evaluation of the air-sea exchange of CO_2 is crucial to determine local and global balances of carbon in the atmosphere-ocean system.

The evaluation of the atmosphere-ocean CO_2 exchange is regulated by the gradient of pCO_2 across the air-sea interface, the gas transfer velocity (or piston velocity), and the solubility of CO_2 in water. There are a few methods available for evaluating the transfer velocity of CO_2 air-sea exchange, which can be obtained by field measurements (*Broecker and Peng*, 1974) or in the laboratory (*Liss*, 1988). Field methods were applied using a variety of data sets obtained from numerous experiments, e.g., Barbados Oceanographic and Meteorological Experiment (BOMEX), Geochemical Ocean Sections Study (GEOSECS), and Transient Tracers in the Ocean (TTO) programs (*Broecker and Peng*, 1971; *Peng et al*., 1974; *Peng et a*l., 1979; *Smethie et al*., 1985; *Batrakov et al*., 1981). Laboratory methods using wind/wave tunnel experiments can be used to relate the wind speeds with the measured transfer velocities (*Liss and Merlivat*, 1986). This was the approach employed in the Programme Français Océan-Climat en Atlantique Equatorial (FOCAL) described by *Andrié et al*. [1986], *Oudot and Andrié* [1986], and *Oudot et al*. [1987]. In addition to the GEOSECS and TTO programs, there are also some studies on the variability of the oceanic CO_2 system in the subarctic Atlantic Ocean (*Takahashi et al., 1983*; *Takahashi et al.,* 1985), the tropical Atlantic Ocean (*Oudot and Andrié* 1989), the western Pacific Ocean (*Fushimi, 1987*; *Inoue et al.,* 1987), the Southern Ocean (*Inoue and Sugimura*, 1988), and the subarctic North Pacific (*Gordon et al.,* 1971; 1973; *Takahashi, 1989*; *Murphy et al.,* 1998).

The seasonal and interannual variations of CO_2 in the surface oceans are not only affected by the air-sea exchange physical processes but also by the photosynthetic uptake of CO_2 by phytoplankton. For instance, spring phytoplankton blooms in the surface waters of the North Atlantic Ocean can cause a precipitous reduction of surface water pCO_2, CO_2 and nutrients in a span of a couple of weeks. The mechanisms that drive this large biogeochemical variability were modeled by previous investigators (for example; *Taylor et al.,* 1991). In contrast, seasonal changes in CO_2 and nutrients are more gradual in the North Pacific and macro-nutrients are only partially consumed in the surface waters of the subarctic North Pacific Ocean (*Takahashi et al.,* 1993).

In this TM, we describe the model functionality and analyze its application to the seasonal and interannual variations of phytoplankton, nutrients, pCO_2, and CO_2 concentrations in the eastern subarctic Pacific at Ocean Weather Station P (OWS P, 50° N 145° W). We use a verified one-dimensional ecosystem model (*McClain et al.*, 1996), coupled with newly incorporated carbon flux and carbon chemistry components, to simulate 22 years (1958-1980) of pCO_2 and CO_2 variability at Ocean Weather Station P (OWS P). This relatively long period of simulation verifies and extends the findings of previous studies (*Wong and Chan*, 1991; *Archer et al*., 1993; *Antoine and Morel*, 1995a; *Antoine and Morel*, 1995b) using an explicit approach for the biological component and realistic coupling with the carbon flux dynamics. The slow currents and the horizontally homogeneous ocean in the subarctic Pacific make OWS P one of the best available candidates for modeling the chemistry of the upper ocean in one dimension. The chlorophyll and ocean currents composite for 1998 shown in Figure 1 illustrates this premise. The chlorophyll concentration map was derived from SeaWiFS data and the currents are from an OGCM simulation (*R. Murtugudde,* personal communication).

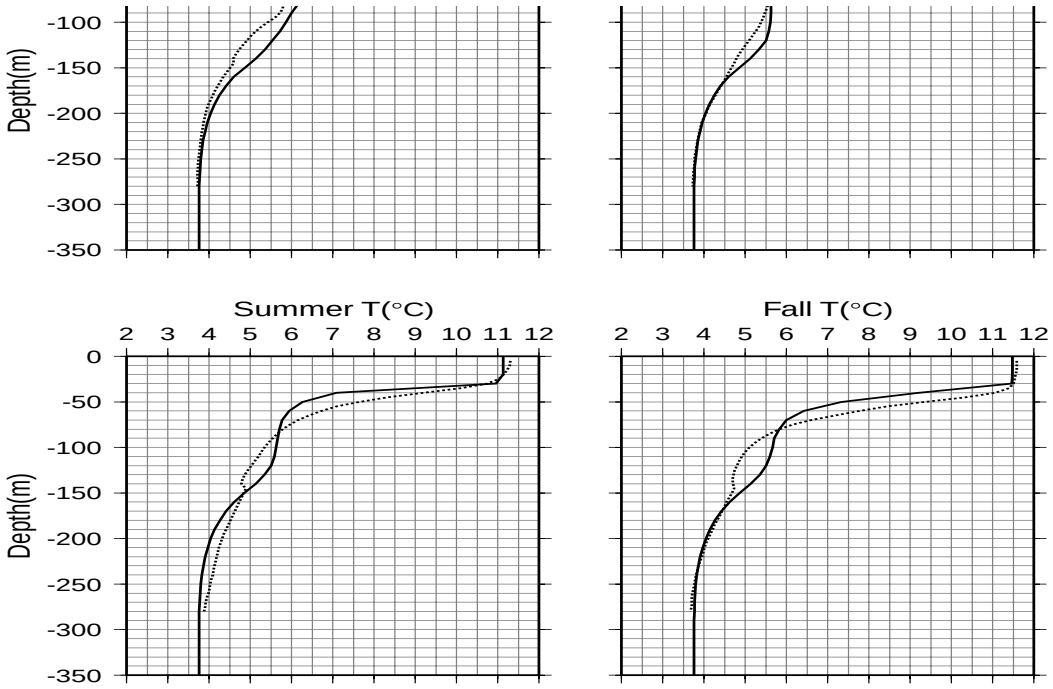

Figure 1. Chlorophyll and ocean currents composite for 1998 based on SeaWiFS data and OGCM simulations, respectively. The black dot denotes the location of OWS P.

TABLE OF CONTENTS

LIST OF FIGURES

LIST OF TABLES

1.0 MODEL DESCRIPTION

The model consists of a previously verified (*McClain et al.*, 1996) four-component ecosystem model, coupled with newly added carbon dioxide and oxygen components. The ecosystem model is physically forced by sea surface temperature (SST) and mixed layer depth values originating from the Garwood mixed layer model (*Garwood*, 1977). A description of the mixed layer model validation and application to the forcing of the ecosystem model is given in *McClain et al.* [1996] and is not reproduced here. The ecosystem model has some modifications which are explicitly defined in *McClain et al*. [1998] and *McClain et al*. [1999]. In addition to these modifications, two new components, iron (Fe) and dissolved organic carbon (DOC), were added to the model. Previous studies (*Maldonado et al.*, 1999; *Boyd et al.*, 1996; *Martin et al.*, 1989) showed that the phytoplankton growth in the subarctic Pacific is generally iron limited. We added the iron component to obtain more accurate simulations of nitrate, phytoplankton and community production. The DOC component was added to more accurately reproduce the seasonality of the net community production via the respiration of DOC by bacteria during the fall-winter period. In addition, the light penetration model uses a different spectral set of water absorption (a_w) coefficients and phytoplankton specific absorption (a^*_p) coefficients. Figure 2 shows the spectral variability of these coefficients. The clear sky irradiance is modified to account for the observed cloud cover by applying a power law correction (*McClain et al.*, 1996) tuned to yield the observed climatological monthly mean surface irradiances (*Dobson and Smith*, 1988). The climatological monthly irradiance, obtained by averaging the daily mean irradiance for each month and for the entire period of simulation (1960-1980), is shown in Figure 3. The seasonal variability shown in Figure 3 agrees with the values given by *Dobson and Smith* [1988]. The coefficient for the cloud attenuation formulation of *McClain et al.* [1996], given by

$$E_o = E_{clear}\,[1\text{-}0.53 Cld^{0.5}] \tag{1}$$

was changed from 0.53 to 0.45 to better match the climatological cloudy sky radiation (E_o) of *Dobson and Smith* [1988]. This new coefficent also provided an improved match of the simulated SST with the observed values. The cloud cover (*Cld*, in oktas) was obtained from OWS P observations.

The following system of coupled differential equations simulates the dynamics of phytoplankton nitrogen (*P*), zooplankton nitrogen (*Z*), ammonium (NH_4), nitrate (NO_3), iron (*Fe*), dissolved organic carbon (*DOC*), total carbon dioxide (CO_2), and oxygen (O_2) stocks within the upper ocean:

$$\frac{\partial P}{\partial t} + w_e \frac{\partial P}{\partial z} + \frac{\partial SP}{\partial z} - \frac{\partial}{\partial z}\left[K_v \frac{\partial P}{\partial z}\right] = GP - mP - r_p P - IZ \tag{2}$$

$$\frac{\partial Z}{\partial z} + w_e \frac{\partial Z}{\partial z} - \frac{\partial}{\partial z}\left[K_v \frac{\partial Z}{\partial z}\right] = (1-\gamma) IZ - (g+hZ)Z - r_Z Z \tag{3}$$

$$\frac{\partial NH_4}{\partial t} + w_e \frac{\partial NH_4}{\partial t} - \frac{\partial}{\partial z}\left[K_v \frac{\partial NH_4}{\partial z}\right] =$$

$$(a_p m + r_p - \pi_1 G)P + [a_z (g+h_z) + r_z + c_{pel}\gamma I]Z - A_n + k_{rc} DOC \frac{N}{C} \tag{4}$$

$$\frac{\partial NO_3}{\partial t} + w_e \frac{\partial NO_3}{\partial z} - \frac{\partial}{\partial z}\left[K_v \frac{\partial NO_3}{\partial z}\right] = -\pi_2 GP + A_n \tag{5}$$

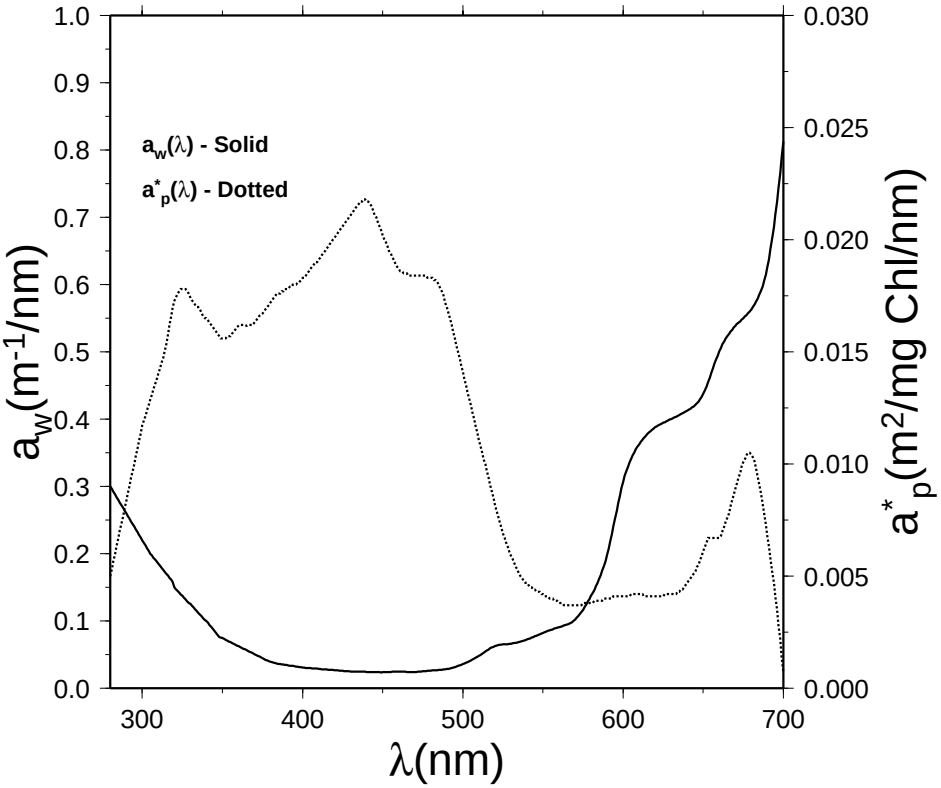

Figure 2. Spectral light absorption coefficient for sea water ($a_w(\lambda)$) and specific chlorophyll absorption coefficient ($a^*_p(\lambda)$) adopted in the spectral downwelling irradiance model formulation.

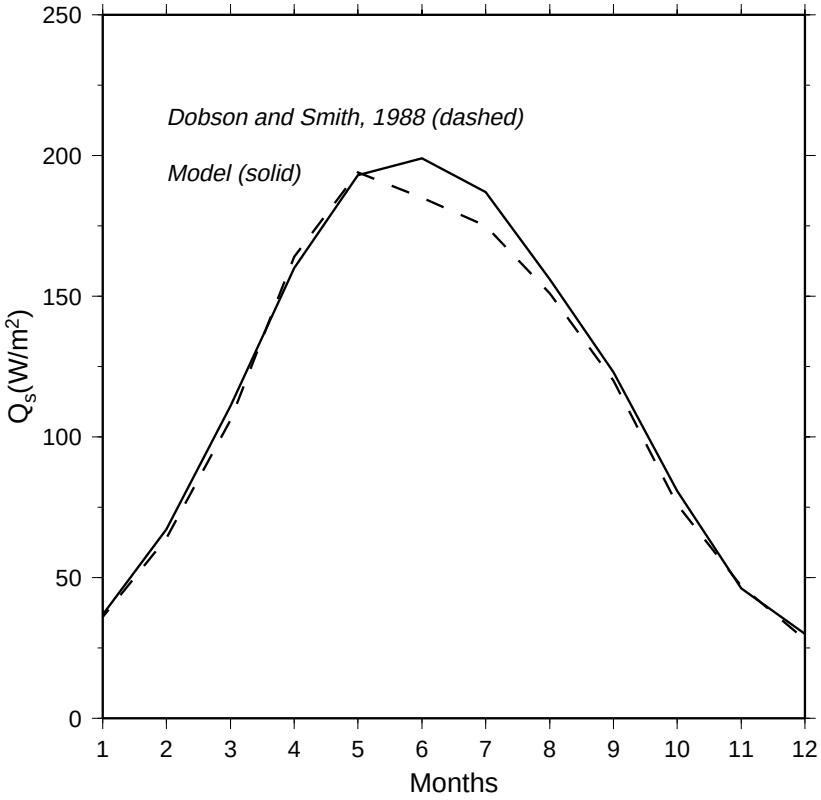

Figure 3. Comparison between the climatological daily averaged cloudy sky surface solar irradiance from *Dobson and Smith* [1988] and model simulation.

$$\frac{\partial Fe}{\partial t} + w_e \frac{\partial Fe}{\partial z} - \frac{\partial}{\partial z}\left[\frac{\partial Fe}{\partial z}\right] = \delta(z)\, FFe - N_p \frac{Fe}{N} \tag{6}$$

$$\frac{\partial DOC}{\partial t} + w_e \frac{\partial DOC}{\partial z} - \frac{\partial}{\partial z}\left[K_v \frac{\partial DOC}{\partial z}\right] = (a'_p mP + a'_z (g + hZ)Z)\frac{C}{N} - k_{rc} DOC \tag{7}$$

$$\frac{\partial TCO_2}{\partial t} + w_e \frac{\partial TCO_2}{\partial z} - \frac{\partial}{\partial z}\left[K_v \frac{\partial TCO_2}{\partial z}\right] = \delta(z)\, FCO_2 - N_p \frac{C}{N} + k_{rc} DOC \tag{8}$$

$$\frac{\partial O_2}{\partial t} + w_e \frac{\partial O_2}{\partial z} - \frac{\partial}{\partial z}\left[K_v \frac{\partial O_2}{\partial z}\right] = \delta(z)\, FO_2 + \left[N_p \frac{C}{N} - k_{rc} DOC\right]\frac{O_2}{C} \tag{9}$$

A flow chart of the coupled model, showing the interaction between its major components, is shown in Figure 4. Table 1 summarizes the parameters used in Equations (2) through (9) and derived quantities. The ratios *C/N*, O_2/C are the carbon-to-nitrogen and oxygen-to-carbon Redfield ratios (106:16, 138:106), respectively. The iron-to-nitrogen ratio is assumed to be 19.8 μmol/mol. The Kroenecker delta (δ[z=0]=1; δ[z>0]=0) is used to denote that the carbon dioxide and oxygen fluxes (FCO_2 and FO_2, respectively) are applied at the air-sea interface only. Details of the Ekman upwelling (w_e) and vertical diffusion (K_v) formulations, the numerical method to solve the coupled differential equations, and the various parameters used by the ecosystem model components are given in *McClain et al*. [1996]. The Ekman upwelling profile function was modified to account for depth attenuation below the Ekman depth (D_e). The formulation for D_e (*Pond and Pickard*, 1978) as a function of wind speed *W* and latitude *f*, the shape function *R(z)*, and the vertical velocity are given by:

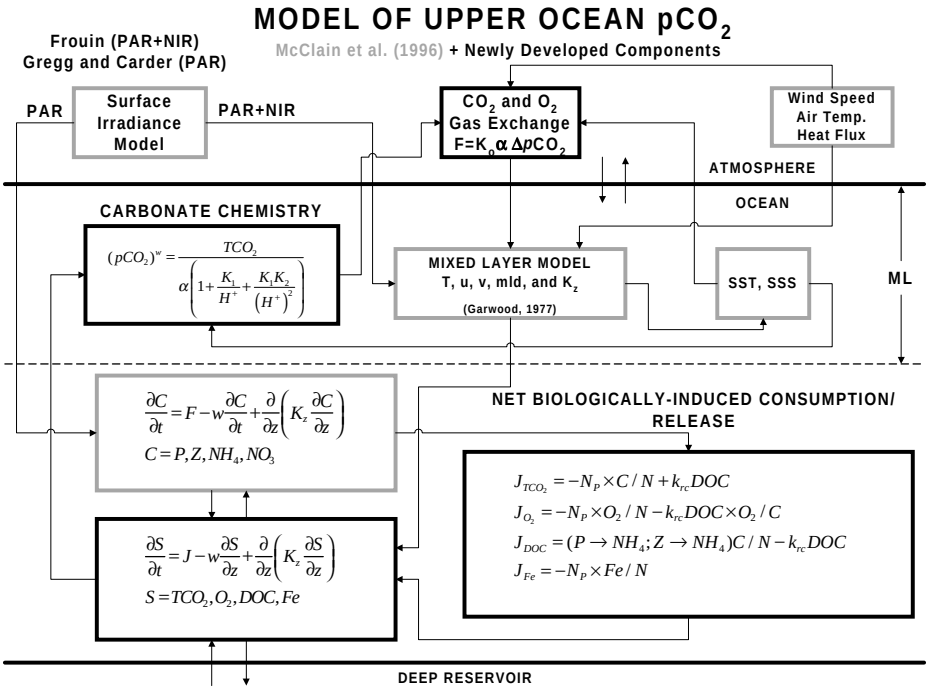

Figure 4. Flowchart showing the principal components of the ecosystem/carbon-flux one-dimensional model.

$$D_e = \pi\left(\frac{2K_v}{f}\right)^{1/2} \tag{10a}$$

$$D_e \approx \frac{4.3W}{[\sin(|\phi|)]^{0.5}} \tag{10b}$$

$$R(z)=\left[1-\cos\left(\frac{\pi z}{2D_e}\right)e^{\frac{-\pi z}{D_e}}\right], \quad for\ z \le D_e \tag{11}$$

$$R(z)=\left[1-\left(\frac{z-D_e}{z_{\max}-D_e}\right)^{1.5}\right]\cos\left[\frac{\pi(z-D_e)}{2(z_{\max}-D_e)}\right], \quad for\ z > D_e \tag{12}$$

$$w_e = w_{D_e} R(z) \tag{13}$$

Equation 10b (*Pond and Pickard*, 1978) produces nearly identical values of D_e as the standard Ekman formula given in Equation 10a. The standard formula introduced numerical instabilities, so Equation 10b was used. The shape function *R(z)* is constructed based on *McClain et al.* [1996] for the portion above D_e (equation 11). For $z > D_e$, *R(z)* is formulated such that continuity at the inflection points $z=D_e$ and $z=z_{max}$ is maintained, and that *R(z)* decreases to zero monotonically towards $z=z_{max}$=350 meters (equation 12).

The net community production, N_p, is defined as the summation of all sources and sinks of nitrate and ammonium in equations (3) and (4):

$$N_p = (a_p m + r_p - G)P + [a_z(g+h_z)+r_z+c_{pel}\gamma I]Z + k_{rc}DOC\frac{N}{C} \tag{14}$$

The ratio *N/C* is 16:106 (Redfield ratio). The effective growth is a function of the maximum growth (G_o), light limitation (L_{lim}), and nutrient limitation (N_{lim}):

$$G = ß\ G_o\ e^{(k_{gp}T)} \tag{15}$$

$$ß = E_{\lim}\min(N_{\lim}, Fe_{\lim}) \tag{16}$$

$$E_{\lim} = 1-\exp\left(-\frac{E_{in}}{Ik_{\max}}\right) \tag{17}$$

$$Fe_{\lim} = \frac{Fe}{(K_{Fe}+Fe)} \tag{18}$$

$$N_{\lim} = NH_4\lim + NO_3\lim \tag{19}$$

$$NO_3\lim = \frac{NO_3}{(K_{NO3}+NO_3)}\frac{(1-NH_4)}{(K_{NH4}+NH_4)} \tag{20}$$

$$NH_4\lim = \frac{NH_4}{(K_{NH4}+NH_4)} \tag{21}$$

2.0 MODEL FORCING AND BOUNDARY CONDITIONS

The Neumann boundary condition, $\partial X/\partial z=0$, is applied at both the surface and lower (350 m) model domain boundaries for *P* and *Z*. Initial profiles of temperature and NO_3 were obtained from winter and annual climatologies (*Conkright, et al.*, 1994), respectively. Depth-independent initial concentrations of *P* and *Z* are 0.2 and 0.1 mmol N m^{-3}, respectively. Observed fall profiles of NH_4 were used as initial conditions (*Frost*, 1993). At the lower boundary, fixed values equal to 0.0 and 41.5 mmol N m^{-3} were applied to NH_4 and NO_3, respectively. The Neumann condition was applied at the surface.

For TCO_2 and O_2, climatological values at the surface and at the bottom were used to construct the initial linear profiles (surface TCO_2=2050 mmol m^{-3} and bottom CO_2=2100 mmol m^{-3}; surface O_2=320 mmol m^{-3} and bottom O_2=100 mmol m^{-3}). A fixed value equal to the initial condition was applied at the lower boundary. The following formulations for the CO_2 and O_2 gas exchanges were applied in the form of flux boundary conditions (FCO_2 and FO_2 in mmol m^{-2} d^{-1}) at the sea-air interface:

$$FCO_2=K_o\alpha\Delta pCO_2 \tag{22}$$

$$FO_2=K_o[O_2(\text{sat})-O_2] \tag{23}$$

$$\alpha = \exp\left[-60.2409+\frac{9345.17}{T}+23.3585\log\left(\frac{T}{100}\right)+S(0.023517-0.023656T+0.0047036T)^2\right] \tag{24}$$

where, *k* is the gas exchange coefficient (piston velocity, in m/d) which is a function of water temperature and wind speed (*Wanninkhof*, 1992; *Liss and Merlivat*, 1986), α is the CO_2 solubility in seawater (in mmol m^{-3} μatm^{-1}) which is a function of temperature and salinity (*Weiss*, 1974), ΔpCO_2 (in μatm) is the difference between air and sea pCO_2, and $O_2(sat)$ is the oxygen saturation concentration (in mmol m^{-3}) in seawater which is a function of temperature and atmospheric pressure (*Weiss*, 1970).

The eolian iron flux, *FFe*, is given by:

$$FFe=\frac{C_{dust}Sc_{Fe}\text{Pr}\,C_{Fe}S_{Fe}}{55.84} \tag{25}$$

where, C_{dust} is the seasonal atmospheric dust concentration in ng/(kg of air) from *Tegen and Fung* [1994], Sc_{Fe}=1000 is the scavenging ratio (Duce, 1995), *Pr* is the daily National Centers for Environmental Prediction (NCEP) precipitation in kg/m^2/d, C_{Fe}=0.035 is the iron mass fraction in the dust, and S_{Fe}=0.1 is the soluble iron fraction. The numerical factors are used to convert dust concentration to an iron flux (*FFe)* in pmol/m^2/d. The seasonal variability of precipitation and the iron flux for the period of 1970-1980 is shown in Figure 5.

Table 1. Summary of model variables and input parameter definitions and values. Initial surface and bottom concentrations are provided when appropriate

Symbol	Value	Definition
P	0.2	Initial phytoplankton concentration (mmol N/m^3)
Z	0.1	Initial zooplankton concentration (mmol N/m^3)
NH_4	0.1	Initial ammonium concentration (mmol N/m^3)
NO_3	Climatology	Initial nitrate concentration (mmol N/m^3)
Fe	50/400	Initial iron concentration (pM)
DOC	10/0	Initial dissolved organic carbon (mmol C/m^3)
TCO_2	2050/2100	Initial total CO_2 Concentration (mmol CO_2/m^3)
O_2	320/100	Initial oxygen concentration (mmol O_2/ m^3)
$\pi 1$		Regenerated production fraction
$\pi 2$		New production fraction
K_{NO3}	0.5	Half saturation for NO_3 uptake (mmol N/m^3)
K_{NH4}	0.1	Half saturation for NH_4 uptake (mmol N/m^3)
K_{Fe}	35	Half saturation for Fe uptake (pM)
I	1	Maximum zooplankton grazing rate (d^{-1})
N_p		Net community production (mmol C/ m^3/d)
m	0.05	Phytoplankton death rate (d^{-1})
G_o	0.5899	Phytoplankton growth rate at 0 ^oC (d^{-1})
k_{gp}	0.0633	Temperature sensitivity of algal growth ($^oC^{-1}$)
η	0.02	Respiration coefficient
k_{rp}	0.0633	Temperature sensitivity of algal resp. ($^oC^{-1}$)
Ik_{max}	50 (<60m)	Maximum photoacclimation param. (μEin/m^2/s)
Ik_{max}	250 (>60m)	Maximum photoacclimation param. (μEin/m^2/s)
pk	5	Ammonium inhibition of NO_3 uptake
S_{max}	1	Maximum phytoplankton sinking Rate (m/d)
Chl-*a*/N	1	Chlorophyll to nitrogen ratio
g	0	Zooplankton death rate (d^{-1})
h	0.35	Quadratic coefficient of zooplankton mortality ($mmol^{-1}$ m^3 d^{-1})
R_m	4	Maximum zooplankton grazing rate (d^{-1})
Λ	0.8	Ivlev constant (m^3/mmol N)
TH	5	Maximum C threshold for Z grazing (mg C/m^3)
γ	0.3	Unassimilated zooplankton ingestion Ratio
r_{zo}	0.019	Respiration rate for zooplankton at 0 ^oC (d^{-1})
k_{rz}	0.15	Temperature sensitivity of Z respiration (d^{-1})
a_p	0.2	Fraction of dead P converted to NH_4
a_z	0.2	Fraction of dead Z converted to NH_4
a'_p	0.1	Fraction of dead P converted to DOC
a'_z	0.1	Fraction of dead Z converted to DOC
k_{rc}	0.01	Respiration rate of DOC into CO_2 (d^{-1})
A^n_{max}	2.0	Maximum rate of nitrification (mmol/d)
D_{min}	0.0095	Minimum inhibition dosage for nitrification (W/m^2)
K_D	0.036	Half saturation dosage for nitrification photoinhibition (W/m^2/nm)
c_{pel}	0.8	Fecal pellet remineralization fraction
K_{vbot}	17.3	Minimum bottom eddy diffusion (m^2/d)

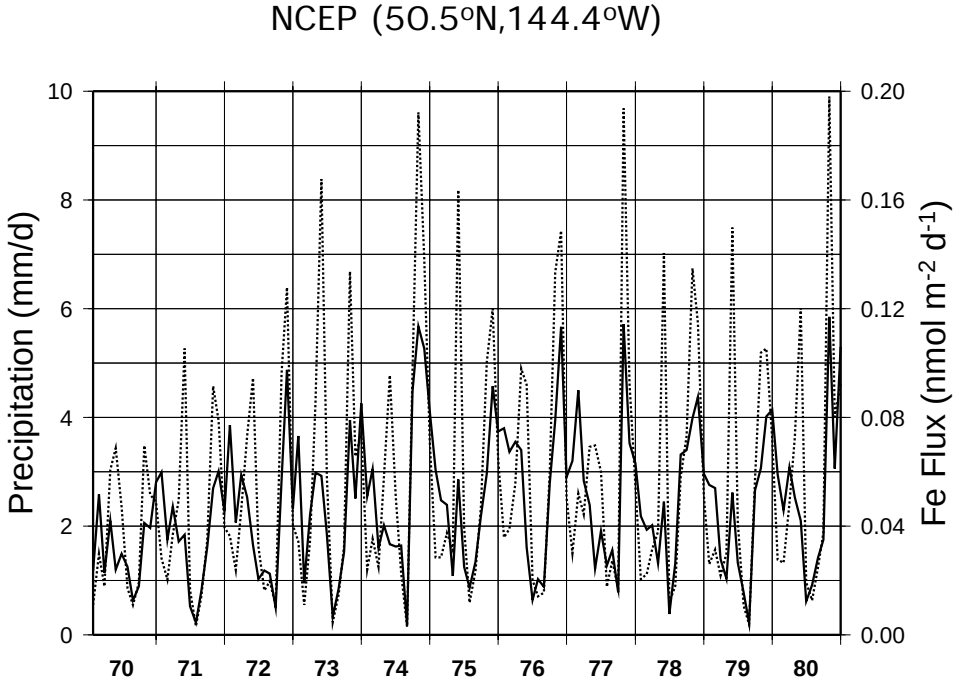

Figure 5.Time series of precipitation rate and eolian iron flux for 1970-1980.

The 30-year pCO_2 atmospheric time series used to force the model is based on a least-squares fit to the 15 years (1978-1993) of pCO_2 observations in Cold Bay, Alaska, the closest long-term monitoring site at roughly the same latitude of OWS P. The pCO_2 time series is given by:

$$pCO_2(air)=A_o+A_1t+A_2\sin\left(\frac{2\pi t}{12}+A_3\right)+A_4\sin\left(\frac{2\pi t}{6}+A_5\right)+A_6\sin\left(\frac{2\pi t}{4}+A_7\right) \quad (26)$$

where t is the time in months, A_0 = 280.8 µatm is the intercept, A_1= 0.134 µatm mo^{-1} is the slope, the amplitudes (A_2, A_4, A_6) are 6.61, 3.01, and 0.87 µatm, respectively. The phases (A_3, A_5, A_7) are 0.77, -15.2, and 0.15 radians, respectively. Figure 6 shows the time series of atmospheric pCO_2 at Cold Bay, at Mauna Loa, and the synthesized signal (dashed line) using the analytical formula (26). Note that the long-term trend at Cold Bay and Mauna Loa are essentially identical, while there is a significant difference in the seasonal amplitudes. The fact that the trends are similar and the amplitudes are different can be attributed to atmospheric mixing processes. Specifically, the atmospheric seasonal mixing is imparted preferentially along latitude lines by virtue of stronger zonal flows in the atmosphere, allowing meridional gradients of pCO_2 to be much stronger than the zonal gradients. Conversely, the long-term trend in pCO_2 distribution is latitudinally more uniform because the meridional mixing time scale is short when compared to the pCO_2 trend due to antropogenic sources.

Sensitivity tests were conducted off-line using the air-sea flux formulation implemented in the model. Four formulations were tested; *Liss and Merlivat* [1986], *Tans et al*. [1990], *Wanninkhof* [1992], and *McGillis and Wanninkhof* [1999]. Monthly averaged (1973-1978) winds, SST, salinity, and ΔpCO_2 from *Wong and Chan* [1991] were used in these calculations. The *Liss and Merlivat* [1986] method provides the smallest sea-air flux (-2.19 mmol CO_2 m^{-2} d^{-1}), whereas the methods of *Tans et al*. [1990] and *Wanninkhof* [1992] provide very similar results (Figure 7). The largest sea-air flux (-31.8 mmol CO_2 m^{-2} d^{-1}) was provided by the *McGillis and Wanninkof* [1999] method since it is a cubic function of the wind speed (W):

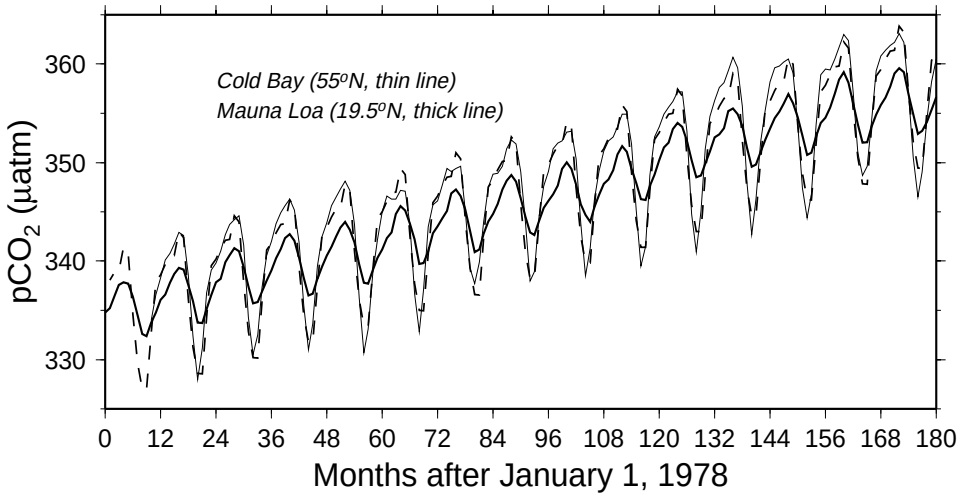

Figure 6. Time series of Mauna Loa and Cold Bay atmospheric pCO_2. The dashed line represents the time series of pCO_2 used to force the model.

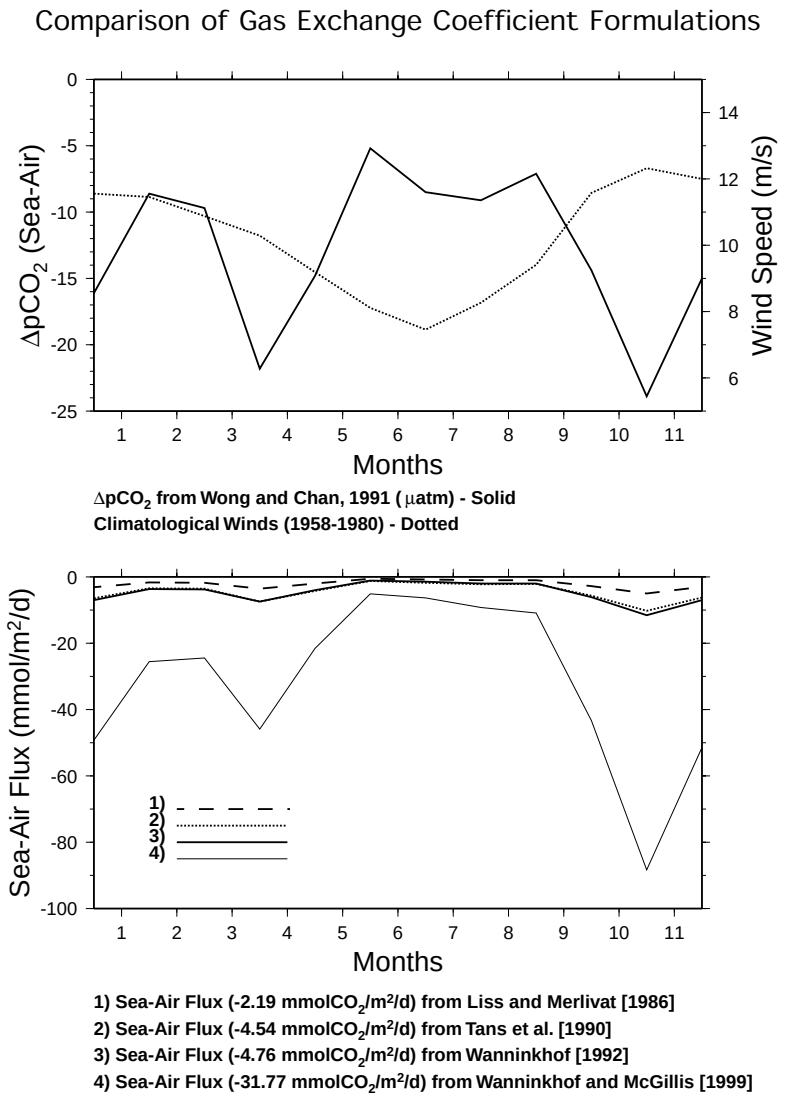

Figure 7. Comparison between sea-air CO_2 flux calculations using four different parameterizations for the gas exchange coefficient.

$$K_o=[1.09W - 0.333W^2 + 0.078W^3]\left(\frac{Sc}{660}\right)^{-1/2} \quad (27)$$

where Sc is the Schmidt number given as a function of temperature T as:

$$Sc = 2073.1-125.62T+3.627T^2-0.043219T^3 \quad (28)$$

Equation (27) is used for the stand-alone flux calculations using climatological winds and various formulations for K. For the actual model simulations we use the formula suggested by *Wanninkhof and McGillis* [1999] for short-term (< 1 day) winds given by:

$$K_o=0.0283W^3\left(\frac{Sc}{660}\right)^{-1/2} \quad (29)$$

We adopted the *McGillis and Wanninkhof*, [1999] method for this study. We conducted several sensitivity runs using different methods to derive the gas exchange coefficient. Figure 8 shows the ΔpCO_2 and air-sea flux seasonal plots simulated by the model for three different gas exchange coefficient methods. The surface CO_2 fluxes obtained with the *Liss and Merlivat* [1986], *Wanninkhof* [1992], and *Wanninkhof and McGillis* [1999] are -6.8, -8.8, and -10.5 mmol/m^2/d, respectively. The negative sign indicates that the flux is from the atmosphere to the ocean in all three cases. We discuss more details of these results in section 4.

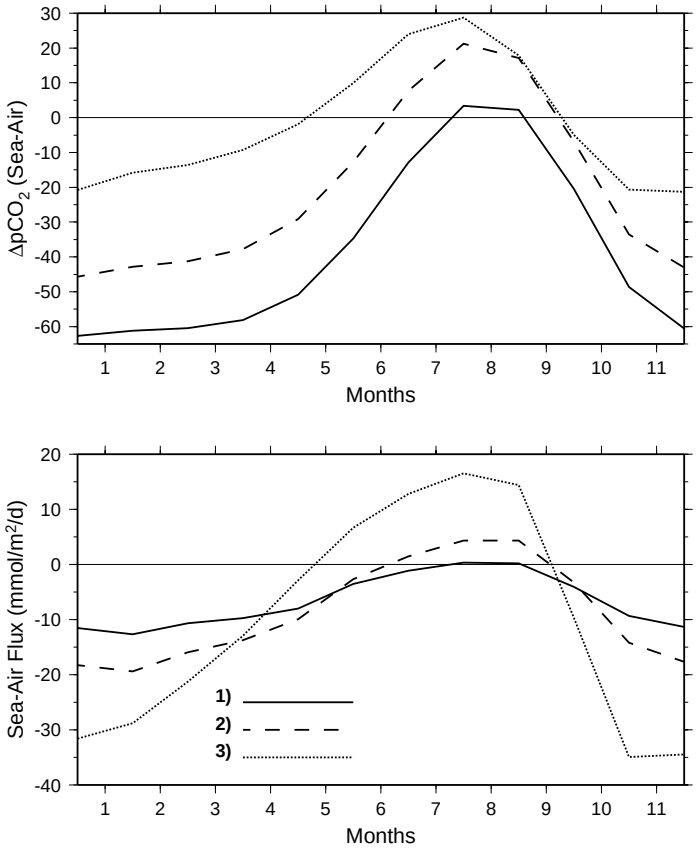

1) Sea-Air Flux (-6.80 mmolCO_2/m^2/d) from Liss and Merlivat [1986]
2) Sea-Air Flux (-8.75 mmolCO_2/m^2/d) from Wanninkhof [1992]
3) Sea-Air Flux (-10.51 mmolCO_2/m^2/d) from Wanninkhof and McGillis [1999]

Figure 8. Seasonal variability of sea-air ΔpCO_2 and surface flux predicted by the model using three different gas exchange formulations.

3.0 OCEANIC pCO_2 FORMULATION

To calculate the pCO_2 concentration in seawater we must first understand the thermodynamics of the CO_2 system. The total CO_2 concentration in seawater, TCO_2, can be written as:

$$TCO_2 = \left[CO_2\right] + \left[HCO_3^-\right] + \left[CO_3^{2-}\right] \tag{30}$$

where all quantities in square brackets are stoichiometric concentrations; $[CO_2]$ is the dissolved carbon dioxide, $[HCO_3^-]$ is the bicarbonate ion, and $[CO_3^{2-}]$ is the carbonate ion. Another quantity that influences the calculation of pCO_2 is the total alkalinity, TA, which can be written as the sum of its major terms:

$$TA = CA + \left[B(OH)_4^-\right] + \left[OH^-\right] - \left[H^+\right] \tag{31}$$

where $CA=[HCO_3^-]+2[CO_3^{2-}]$ is the carbonate alkalinity, $[B(OH)_4^-]$ is the borate ion concentration, and $[OH^-]$ and $[H^+]$ are the products of H_2O dissociation. The partial pressure of dissolved CO_2 is defined by the relationship:

$$pCO_2 = \frac{[CO_2]}{\alpha} \tag{32}$$

where $[CO_2]$ represents the carbon dioxide in solution and α (mmol m^{-3} μatm^{-1}) is the solubility of carbon dioxide in seawater (Weiss, 1974). We can calculate $[CO_2]$ from TCO_2 and TA (the values for the hydrogen ion activity, H^+, and the carbonate alkalinity, CA, are also computed). We follow the recursive formulation of *Antoine and Morel* [1995] to estimate the dissolved $[CO_2]$ concentration

$$[CO_2] = TCO_2 - A + \left[\frac{AK_r - TCO_2K_r - 4A + Z}{2(K_r - 4)}\right] \tag{33}$$

where A takes the value of TA initially. K_r is equal to K_1/K_2, where K_1 and K_2 (mmol m^{-3}) are the dissociation constants of carbonic acid, which are a function of temperature and salinity (*Goyet and Poisson*, 1989). The other quantities required to calculate $[CO_2]$ are

$$Z = \sqrt{(TCO_2K_r)^2 + AK_r(2TCO_2 - A)(4 - K_r)} \tag{34}$$

$$H^+ = \frac{([CO_2]K_1)}{2A} + \sqrt{\frac{([CO_2]K_1)^2 + 8A[CO_2]K_1K_2}{2A}} \tag{35}$$

$$CA = TA - BR\frac{K_B}{K_B + H^+} - \frac{K_w}{H^+} + H^+ \tag{36}$$

$$K_1 = 10^{-pK_1}, K_2 = 10^{-pK_2} \tag{37}$$

$$pK_1 = \frac{812.27}{T} + 3.356 - 0.00171\,S\log(T) + 0.000091\,S^2 \tag{38}$$

$$pK_2 = \frac{1450.87}{T} + 4.604 - 0.00385\,S\log(T) + 0.000182\,S^2 \tag{39}$$

$$K_w = 10^{-pK_w} \tag{40}$$

$$pK_w = \frac{3441}{T} + 2.241 - 0.09415\, S^{0.5} \tag{41}$$

$$\ln(K_B) = \frac{-8966.9 - 2890.53S^{0.5} - 77.942S + 1.728S^{1.5} - 0.09963S^2}{T} +$$
$$148.0248 + 137.1942S^{0.5} + 1.62142S +$$
$$(-24.4344 - 25.085S^{0.5} - 0.2474S)\log(T) + 0.053105TS^{0.5} \tag{42}$$

where $BR = 0.00042S/35.0$ mmol m^{-3} is the borate concentration (*Whitfield and Turner*, 1981), and K_B and K_W are the dissociation constants for boric acid and sea water, respectively (*Weiss*, 1974).

The above equations are repeated, with the variable A taking the value of CA at the previous iteration, until $|CA - A| \le 10^{-8}$. The value of pCO_2 is then estimated according to:

$$pCO_2 = \frac{TCO_2}{\alpha\left(1 + \frac{K_1}{H^+} + \frac{K_1K_2}{H^{+2}}\right)} \tag{43}$$

Table 2 shows a comparison between pCO_2 values measured at OWS P (*Wong and Chan*, 1991) and those calculated using equations (33) through (44). The data were acquired during the winter of 1975 (17 January and 9 February). A very close agreement (less than 1%) is achieved between the observed and calculated pCO_2 values.

Table 2. Oceanic properties of surface sea water from OWS P in early 1975 (*Wong and Chan*, 1991). The measured (a) *pCO2* values are compared with those calculated (b) using equations (30) through (43). The difference between measured and calculated values (ε) is 2.1 μatm

Date	*SST*	*SSS*	*TA*	*TCO2*	pCO_2^a	pCO_2^b	ε
17 Jan	5.8	32.656	2216	2039	312.6	310.5	-2.1
9 Feb	5.8	32.678	2203	2030	317.4	315.3	-2.1

Data collected during 1973-1978 (*Wong and Chan*, 1991) were used to validate and formulate model parameters. The salinity data is much sparser so that an analytical formulation must be obtained to provide an uninterrupted sequence of values to force the model. A regression of salinity versus temperature yields the linear relationship $S = 32.8124 - 0.01719T$. The total alkalinity can be expressed as a linear function of salinity. For example, the linear formulation for *TA* of *Clayton et al.* [1995], with an intercept adapted to reproduce the mean *TA* values at OWS P, can be used to produce an hourly time series of *TA* values to force the model ($TA = 117.8 + 64.232S$). However, since the salinity at OWS P does not change significantly (32.59 to 32.72 psu), the model results are not significantly different than assuming a constant value for *TA*. Also, there is little information available on the seasonal variability of *TA* at OWS P for model verification. Therefore, we used a constant value of 2215 μeq/kg, which is also the value used by *Antoine and Morel* [1995b], and calculated at OWS P in January 1975 by *Wong and Chan* [1991]. Table 3 summarizes the parameters used in the geochemical portions of the model (iron flux and carbonate chemistry).

Table 3. Summary of parameters used in the iron flux formulation and carbonate chemistry

Symbol	Value	Definition
C_{dust}	Climatological	Atmospheric dust concentration (μg/kg of air)
Sc_{Fe}	1000	Iron scavenging ratio
C_{Fe}	0.035	Iron mass fraction
S_{Fe}	0.1	Soluble iron fraction
K_o	Eqs. 27, 29	Gas exchange coefficient
Sc	Eq. 28	Schmidt number
TA	2215	Total Alkalinity (μeq/kg)
$[CO_2]$	Eq. 33	Carbon dioxide in solution (mmol/kg)
pCO_2	Eqs. 32, 43	Partial pressure of CO_2 in sea water (μatm)
α	Eq. 24	CO_2 solubility in sea water (mmol/m^3/μatm)
CA	Eq. 36	Carbonate alkalinity (μeq/kg)
K_1, K_2	Eq. 37	Dissociation constants for carbonic acid
K_B, K_w	Eqs. 40, 42	Dissociation constants for borate and water
BR	0.00042*S*/35	Borate concentration (mmol/m^3)
H^+	Eq. 35	Hydrogen ion concentration

4.0 MODEL SKILL ASSESSMENT

4.1 Model Sensitivity to Forcing and Parameterization

Table 4 shows a summary of the model response to different forcing and parameterization. We provide a comparison between the model results and available data sets from OWS P in the next sub-section. An additional parameter test was performed to evaluate the sensitivity of the carbon dioxide variables to changes in salinity. One of the objectives of this test is to evaluate the required sensitivity and accuracy of salinity remote sensors so that measurements can be useful in the determination of the surface carbon flux in the ocean.

Table 4. Summary of model sensitivity to different parameterizations. The criteria for improvements include agreement with data such as phytoplankton (P) concentration, primary productivity (PP), and pCO_2

Parameter	Range	Result
R_m	3.0-5.0	4.0 for best P, PP
g	Linear to quadratic	$g=0.35Z^2$ for best P, PP
Fe, DOC	Added components	Improved PP seasonality
$a_w(\lambda)$ and $a^*_p(\lambda)$	For OWS P and Warm Pool	Values for OWS P were used
$E_o(\lambda)$	Up to 14% adjustment	Improvement in SST
Gas exchange $K_o(W^2)$	1, 2, and 4xWanninkhof	4x best pCO_2 variability
$K_o(w^3)$	$K_o=(0.0283W^3)(Sc/660)^{-0.5}$	Best agreement with observed pCO_2
pCO_2 calculation from SST, S, TA and TCO_2	Antoine and Morel (1995), P.Murphy (personal communication), DOE	All within less than 5%
TCO_2 (350m)	Constant to seasonal	TCO_2=2100 best profile
CO_2 flux (FCO_2) forcing	Top layer, distributed within mixed layer (ML)	ML approach required for stability (large K_o only)
Iron flux (FFe) forcing	S_{Fe}=0.05,0.1,0.2,0.3	Best P, PP with S_{Fe}=0.05
Carbon Production	Cloern et al. (1995), Redfield Ratio	Redfield Ratio more internally consistent

We use the relationship of *Millero et al.* [1998], which depends on temperature (T) and salinity (S), to calculate the total alkalinity (TA) at each model time step

$$NTA = 2300\text{-}7.00(T\text{-}20)\text{-}0.158(T\text{-}20)^2 \quad (44)$$

$$TA = NTA\frac{S}{35} \quad (45)$$

where NTA is the salinity normalized alkalinity. The salinity is calculated from the regression on temperature based on the salinity and temperature data from OWS P

$$S = 32.8124\text{-}0.01719T \quad (46)$$

We conducted two runs, one using the salinity derived from equation (46), and another using the salinity in equation (46) with a positive bias of 0.5 psu. We adopted the gas exchange coefficient of *Wanninkhof and McGillis* [1999] in both runs. The results are summarized in Table 5. The parameters that are most sensitive to the salinity variability are the ΔpCO_2, and, consequently, the air-sea CO_2 flux. These are also the two variables with standard deviations larger than the mean. The dissolved CO_2 does not change much (< 1%). The 24.3% increase in CO_2 uptake from the atmosphere, due to the 0.5 psu increase in salinity, is compensated by an approximately equivalent decrease in the CO_2 supply via the bottom flux.

Note that the climatological ΔpCO_2 mean is reduced with the increased salinity, but the surface air-sea flux into the ocean actually increases despite the very small change in the gas exchange coefficient. This result seems counter-intuitive at first glance but becomes clear after inspection of the seasonal variations of ΔpCO_2 and K. Figure 9 shows the seasonal variability of the surface CO_2 flux, ΔpCO_2 and K. The solid and dashed lines represent results from runs 1 and 2, respectively. The K values for the two runs are virtually identical. Figure 9 clearly shows that the ΔpCO_2 is largely positive from May through September and negative during the rest of the year. However, K is largest during the winter, spring and fall vigorous wind forcing, but significantly reduced during May through August when the wind speeds subside at OWS P. This phase opposition of ΔpCO_2 and K explains why the surface flux increases despite a climatological decrease in the ΔpCO_2 mean value. Note also that the ΔpCO_2 from Run 2 is more negative during winter, spring and fall than the ΔpCO_2 from Run 1.

Table 5. Summary of sensitivity run based on a 0.5 psu salinity increase from Run 1 to Run 2. The averages are based on years 1960-1980

	Run 1	**Run 2**	**Difference**	**Percent**
S(psu)	32.67	33.17	0.5	1.5
TCO₂(μmol/kg)	2007.1 ± 22.7	2033.1 ± 22.6	26.0	1.3
pCO₂(μatm)	315.6 ± 23.5	314.2 ± 24.4	-1.4	0.5
FCO₂(gC/m²/yr)	-42.4 ± 47.9	-52.7 ± 55.6	-10.3	24.3
Bottom CO₂ Flux (gC/m²/yr)	-25.1 ± 8.2	-15.8 ± 5.5	9.31	37.0
TA(μeq/kg)	2201.2 ± 11.4	2234.9 ± 11.5	33.69	1.5
CO₂(μmol/kg)	14.8 ± 0.9	14.7 ± 0.9	-0.11	0.7
α(mmol/kg/atm)	47.13 ± 3.98	47.0 ± 4.00	-0.13	0.3
ΔpCO₂(μatm)	3.58 ± 26.77	2.15 ± 27.75	-1.43	39.9
K(mmol/m²/d/μatm)	1.376 ± 2.752	1.372 ± 2.744	-0.004	0.3

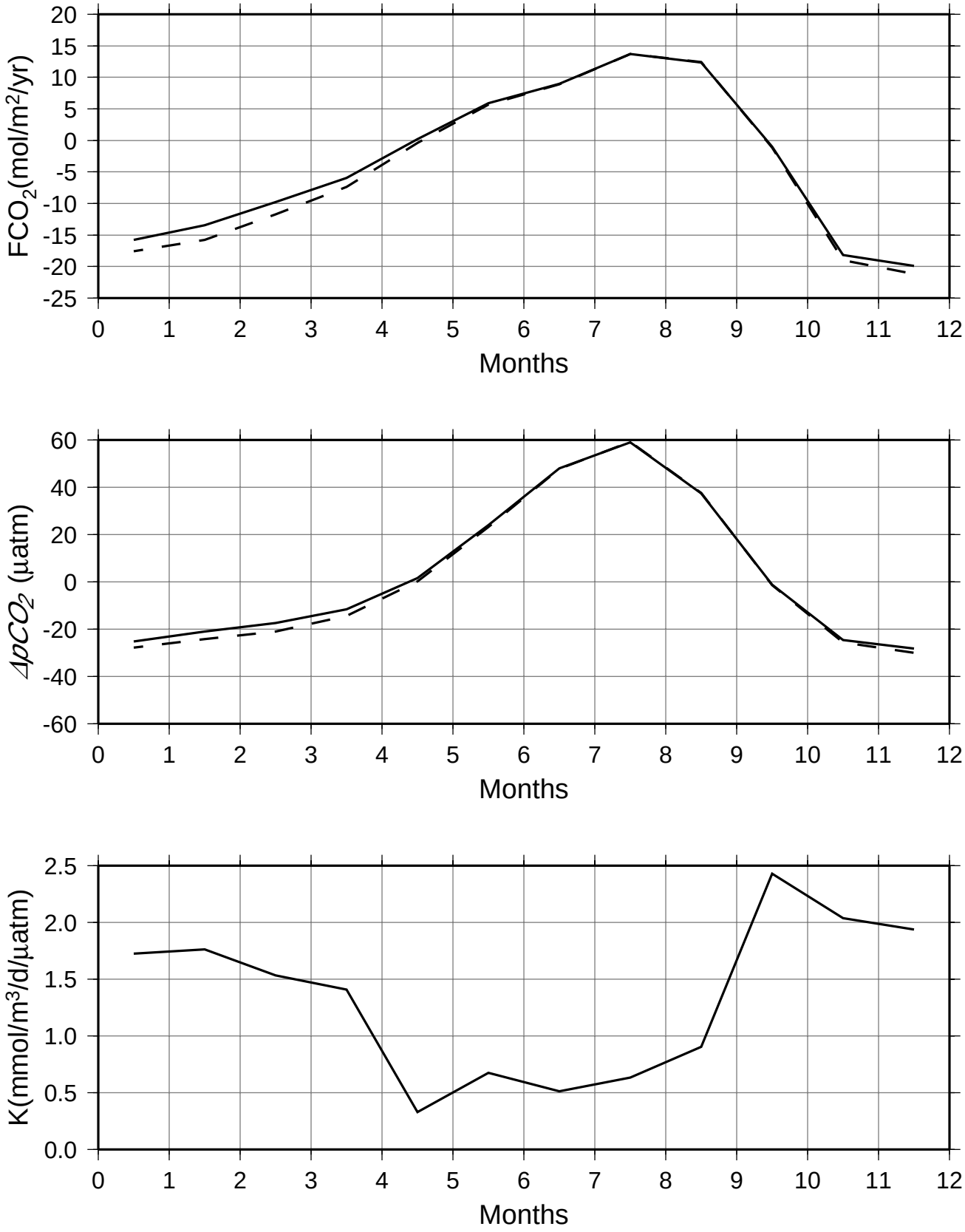

Figure 9. Seasonal variability surface flux, sea-air ΔpCO_2, and gas exchange coefficient predicted by the model for two runs with a salinity difference of 0.5 psu.

4.2 Model-Data Comparison

Table 6 provides a comparison between model and observed (*Wong and Chan*, 1991) biogeochemical parameters. Both model and observed values are averaged over years 1973-1978. Primary production, chlorophyll and nitrate are depth-averaged (0-80 m). This particular model run uses the gas exchange coefficient (K_o) from *Wanninkhof* [1992]. The model primary production is within 20% of the observed value. Chlorophyll, nitrate, and SST are all within less than 5% of the observed values. The salinity is obtained via a regression with SST; thus it is not independent of the observations and should not be evaluated as a model parameter. A comparison between model (solid line) and observed (dotted line) seasonal temperature profiles, averaged over the overlapping model-data years (1958-1966), is shown in Figure 10. The agreement is quite good. The model profiles represent the seasonal variability of the temperature stratification and SST at OWS P reasonably well. A very small warming trend (0.001 °C/month not shown here) was identified below 175 meters (below the euphotic zone). We removed the trend after the fact for display purposes only. These small discrepancies do not significantly affect the model results.

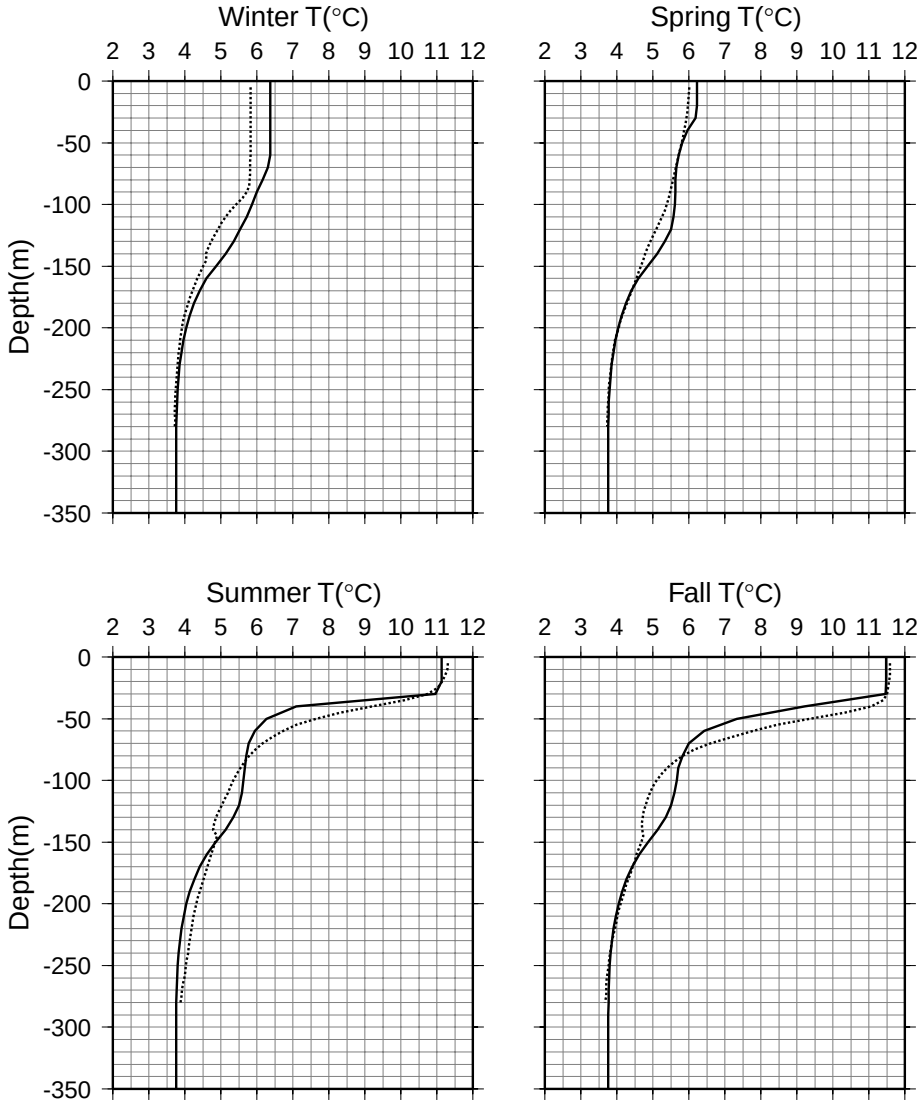

Figure 10. Comparison between model and observed seasonal temperature profiles averaged over the period of 1958-1966.

The model TCO_2 is about 2% lower on average than the observed TCO_2. The mean atmospheric pCO_2 is within 3% of the measured mean. The largest uncertainty lies in the calculation of the air-sea CO_2 flux (FCO_2). The surface flux is the most elusive quantity in the oceanic CO_2 measurements and modeling. It depends on accurate measurements of ΔpCO_2 and a robust formulation for the gas exchange coefficient (K_o), since direct measurements of the air-sea flux are not yet available. As we have shown in section 2, there are multiple gas exchange coefficient formulations in the literature which yield a wide range of values for a given wind speed. For example, as shown in Table 7, FCO_2 can change significantly depending on which formulation for K_o is used. The value calculated from the observed ΔpCO_2 and K_o from *Liss and Merlivat* [1986] is -8.3 gC/m^2/yr; if K_o from *Wanninkhof* [1992] is used the flux increases to -19.1 gC/m^2/yr. Alternatively, the flux calculated by the model using K_o from *Wanninkhof and McGillis* [1999] is -38.1 gC/m^2/yr. In view of this wide range of calculated values, we decided to conduct a series of sensitivity runs with the model to assess the effects of different formulations for K_o.

We conducted 7 sensitivity runs:

(1) baseline run with the best parameter set for the biology components (shown in Table 4) and K_o from *Wanninkhof* [1992];
(2) same run as in (1) except for using K_o from *Liss and Merlivat* [1986];
(3) same run as in (1) except for doubling K_o;
(4) same run as in (1) except for quadrupling K_o;
(5) same run as in (4) except for no iron;
(6) same run as in (4) except for removal of biological drawdown of CO_2 (abiotic); and,
(7) same run as in (1) except for K_o from *Wanninkhof and McGillis* [1999].

The results are summarized in Table 7. A comparison between the sensitivity runs for K (runs 1, 2, 3, 4, and 7) reveals that, as K increases, ΔpCO_2 decreases accordingly but FCO_2 increases much more slowly. For example, the mean values for K, ΔpCO_2, and FCO_2 from run 1 are 0.34, -20.4, and -38.1. Conversely, the mean values for K, ΔpCO_2, and FCO_2 from run 7 are 1.287, -2.3, and -45.6, respectively. Thus, for run 7, K is about 4 times larger, ΔpCO_2 is 9 times smaller, but FCO_2 is only 20% larger. This means that there is a dynamic negative feedback in the model that prevents the surface flux from assuming unrealistically large values no matter how large the value of K is. Table 4 also shows that the iron and the biological uptake affect the surface flux significantly. The run without iron limitation (run 5) provides a surface flux 30% larger, whereas the abiotic run (run 6) reverses the flux direction to +15.8 gC/m^2/yr. The question that still remains is what formulation for K provides the most realistic pCO_2 variability. The relative influence of light and nutrient limitation on the phytoplankton growth simulated by the model is shown in the climatological vertical profiles of light limitation (L_{lim}), nitrate and ammonium limitation (N_{lim}), and iron limitation (Fe_{lim}) of Figure 11. Within the top 50 meters iron is the limiting factor, while below 50 meters, and within the euphotic zone, light is the limiting factor.

Figure 12 shows the seasonal variations of SST, SSS, nitrate, chlorophyll, total carbon dioxide, in situ pCO_2, and pCO_2 normalized to 10 ^{o}C obtained from the model simulation (solid lines) and from observations (black circles and triangles). The chlorophyll data consist of two sources. The *Wong and Chan* [1991] data for the period of 1973-1978 (triangles), and the National Oceanic Data Center (NOAA/NODC) data set for the period of 1959-1980 (circles). All parameters simulated by the model are in good agreement with observations, except for the pCO_2.

Table 6. Comparison between model and observed parameters

	Model	Data
PP ($gC/m^2/yr$)	168	140
Chlorophyll (mg/m^3)	0.33	0.41^{I} 0.32^{II}
Nitrate (μM)	10.8	10.6
SST (^oC)	7.8	8.2
SSS (psu)	32.68	32.67
TCO_2 ($mmol/m^3$)	2016.1	2059.7
Air pCO_2 (μatm)	320.9	329.8
Ocean pCO_2 (μatm)	300.5	317.0
ΔpCO_2 (μatm)	-20.4	-12.8
K ($mmol/m^2/\mu atm/d$)	0.340	0.137^{III}
FCO_2 ($gC/m^2/yr$)	-38.1	-8.3^{III} -19.1

I. From *Wong and Chan* [1991]
II. From *McClain et al.* [1996]
III. Calculated quantities based on wind speed, CO_2 solubility, and ΔpCO_2. Values using K from *Liss & Merlivat and Wanninkhof*, respectively.

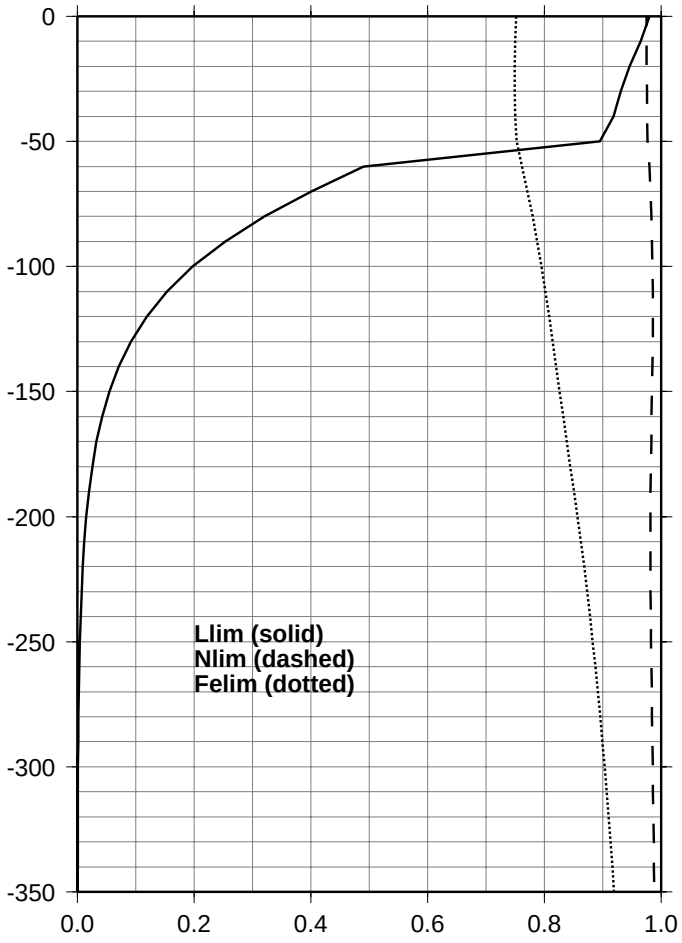

Figure 11. Climatological profiles of light and nutrient limitation predicted by the model.

Table 7. Comparison between 7 different model runs. All values were obtained by averaging the model-data overlapping years (1973-1978), except for the last run (K from *Wanninkhof and McGillis*, 1999) where 21 years (1960-1980) were used for the averages. The first 2 spin-up years (1958-1959) were eliminated from the averages

Run Type	PP ($gC/m^2/yr$)	Chl-a (mg/m^3)	NO_3 (μM)	Ocean pCO_2 (μatm)	TCO_2 ($mmol/m^3$)	ΔpCO_2 (μatm)	$K=K_o\alpha$ ($mmol/m^2/\mu atm/d$)	FCO_2 ($gC/m^2/yr$)
Baseline1	168	0.33	10.8	300.5	2016.1	-20.4	0.340	-38.1
Baseline2	168	0.33	10.8	282.3	2005.4	-38.6	0.156	-29.6
$2xK_o$	168	0.33	10.8	311.4	2022.5	-9.5	0.679	-42.7
$4xK_o$	168	0.33	10.8	317.0	2025.0	-3.9	1.358	-44.4
No iron	198	0.35	4.6	314.6	2023.8	-6.3	1.358	-57.3
Abiotic	0	0	38.8	329.7	2028.3	7.7	1.385	15.8
$K_o(W^3)$	174	0.33	10.8	318.6	2023.1	-2.3	1.287	-45.6

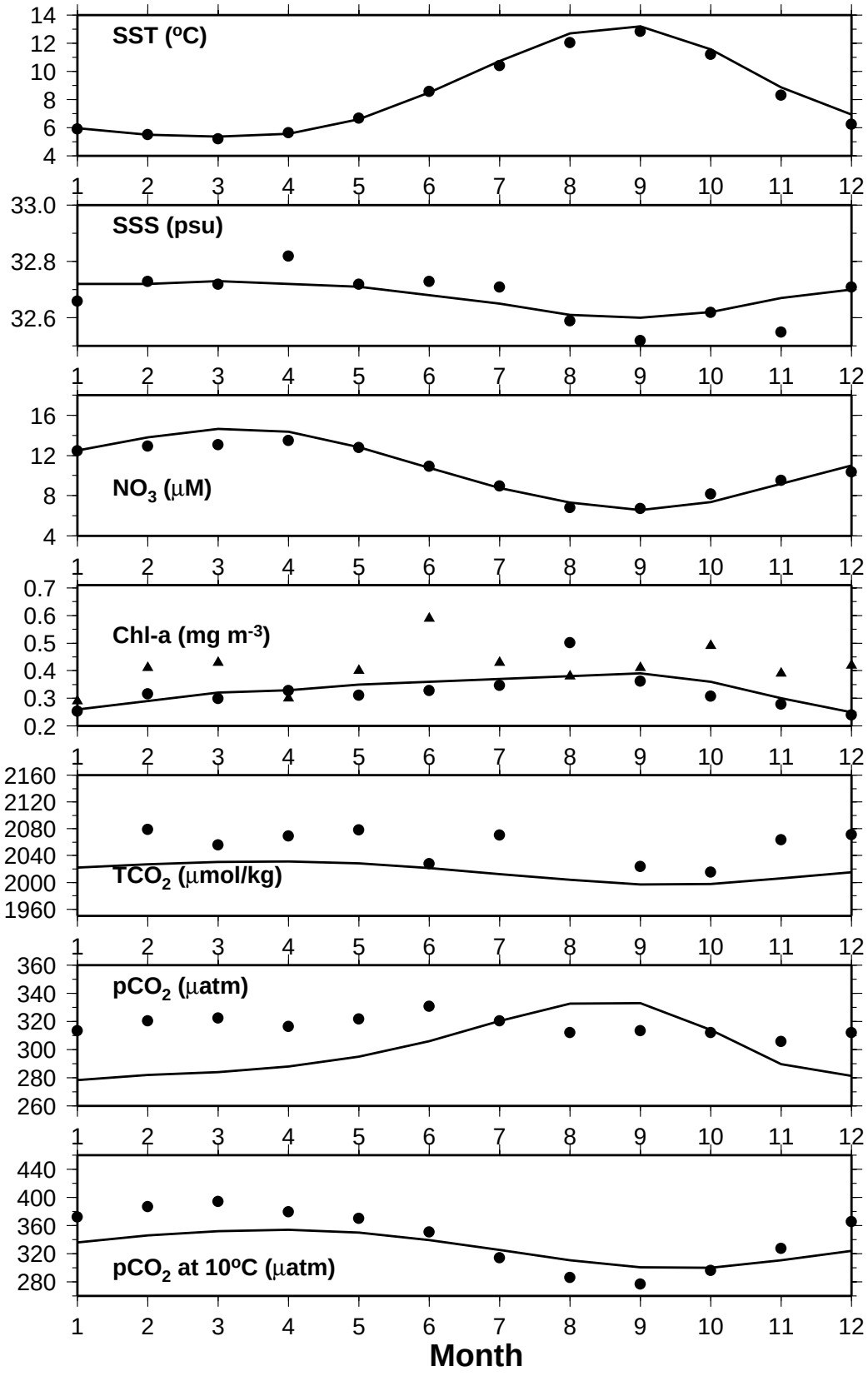

Figure 12. Model (solid line) versus observed (black circles and triangles) seasonal variability of sea surface temperature and salinity, nitrate and chlorophyll averaged over the upper 80 meters, surface total carbon dioxide, pCO_2 at in situ temperature, and pCO_2 normalized to 10 ºC. The gas exchange coefficient of *Wanninkhof* [1992] was used in this simulation.

The model pCO_2 is up to 40 μatm lower in the winter-spring months and about 20 μatm higher in the summer. A significant improvement is achieved when the *McGillis and Wanninkhof* [1999] formulation for K is used. Figure 13 shows the improved results. Note that the pCO_2 seasonal variability is now much closer to the observed data. Figure 14 compares the model and observed pCO_2 interannual variability for the period of 1973-1974. Predictions from run 1 (dotted line) and run 7 (solid line) are shown together with the observed values (solid black circles). It is quite evident that more realistic amplitude and phase of the seasonal cycle are achieved when the *McGillis and Wanninkhof* [1999] formulation for K is used. Therefore we adopted this K formulation for our interannual run. The results of the interannual run are discussed in the following sections.

5.0 SEASONAL VARIABILITY

Figures 15, 16, and 17 show the seasonal variability (from 1960-1980 monthly averages) of the physical and biogeochemical model parameters. These are the vertical velocity, vertical eddy diffusivity, temperature, photosynthetically available radiation (PAR), nitrate, ammonium, zooplankton, phytoplankton, total carbon dioxide, oxygen, and iron. The vertical velocity is very weak in general (maximum of 3 cm/d) with upwelling peaks in the spring and fall when the wind curl is largest. Maximum downwelling occurs in December. The vertical advection effects are minimal when compared to vertical diffusion (K_v). Maximum surface K_v values ranging from 900 to 1000 m^2/d occur in late fall and winter. The depth penetration of large K_v values follows the seasonal changes of the mixed layer depth; largest in winter (120 m) and smallest in summer (20-40 m). Downwelling light intensity and penetration are larger during April-August, peaking in May-June. The warmer temperatures are confined to the top 50 meters and the time period of May-October, with a peak in August-September. The seasonal variability of phytoplankton, nitrate and iron are strongly correlated with top 50-meter peaks extending from May through October. This is consistent with photosynthetic consumption of nutrients during the high growth season. Total carbon dioxide and oxygen are strongly correlated with temperature due to the strong dependence of solubility on temperature.

Oxygen anomalies relative to the temperature-determined saturation value (Figure 18) show that there is a seasonal cycle of air-sea flux, with ingassing in winter and outgassing in summer. The oxygen anomaly in the abiotic case is consistently less than in the full coupled model, suggesting that net community production (N_p) is positive at all times of the year. The biologically generated anomalies contribute very little to the air-sea flux of oxygen. The difference between the biotic and abiotic cases is greatest in summer, with a maximum of 3.3 μM in July, reflecting the seasonal cycle of N_p. This summer maximum in the NetCP was hypothesized by *Wong and Chan* [1991] to explain the absence of a strong seasonal supersaturation of pCO_2. The oxygen supersaturation in the summer months is 1.9-2.8 times the value expected from thermal forcing alone. This is consistent with the oxygen supersaturations determined by *Emerson et al.* [1993], which range from 1.4-2.6 times the values for argon (an inert tracer of abiotic effects on oxygen), so rates of biological new production in the model are reasonable and even on the high side.

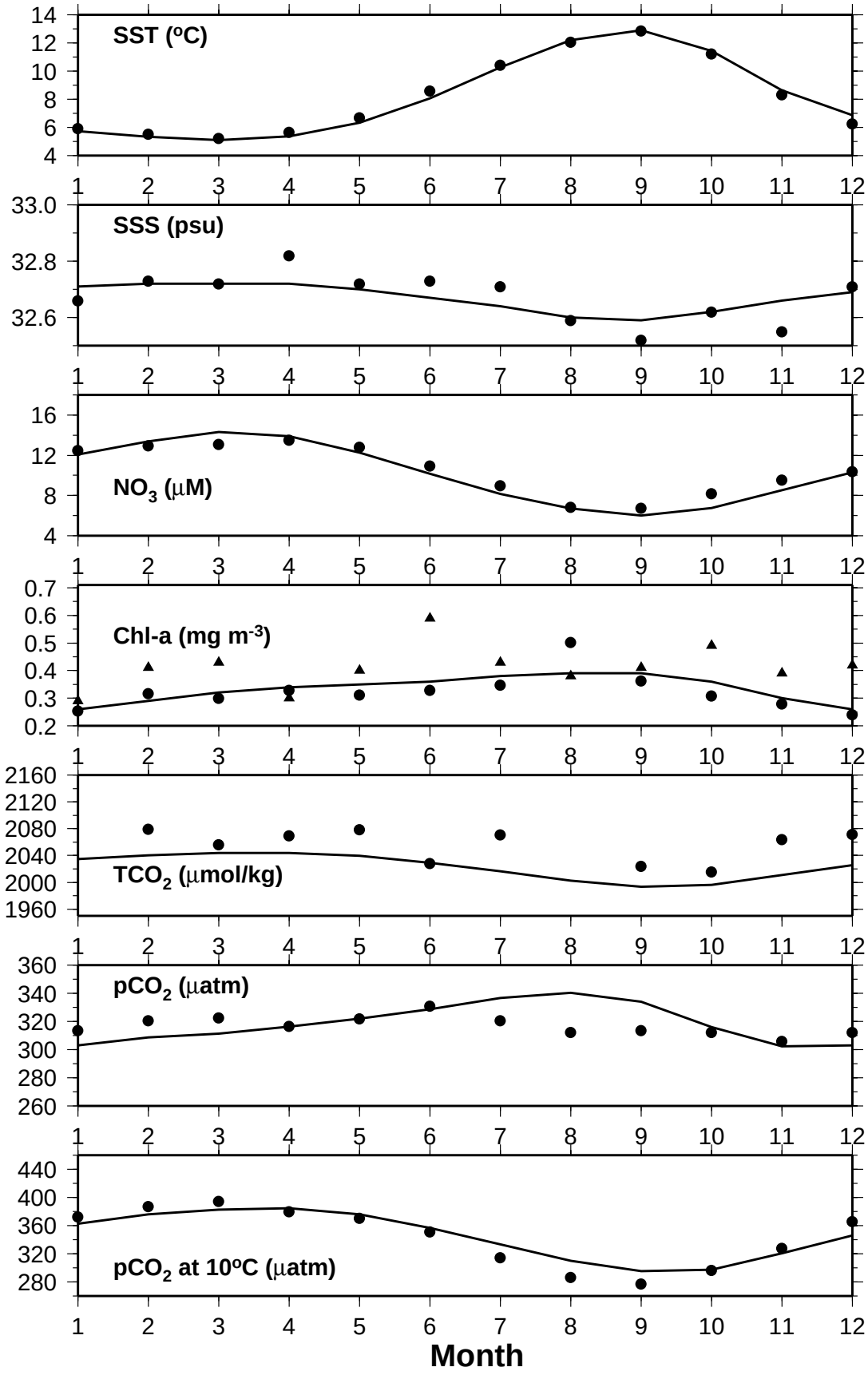

Figure 13. As in Figure 12, except that the gas exchange coefficient of *Wanninkhof and McGillis* [1999] was used in this simulation.

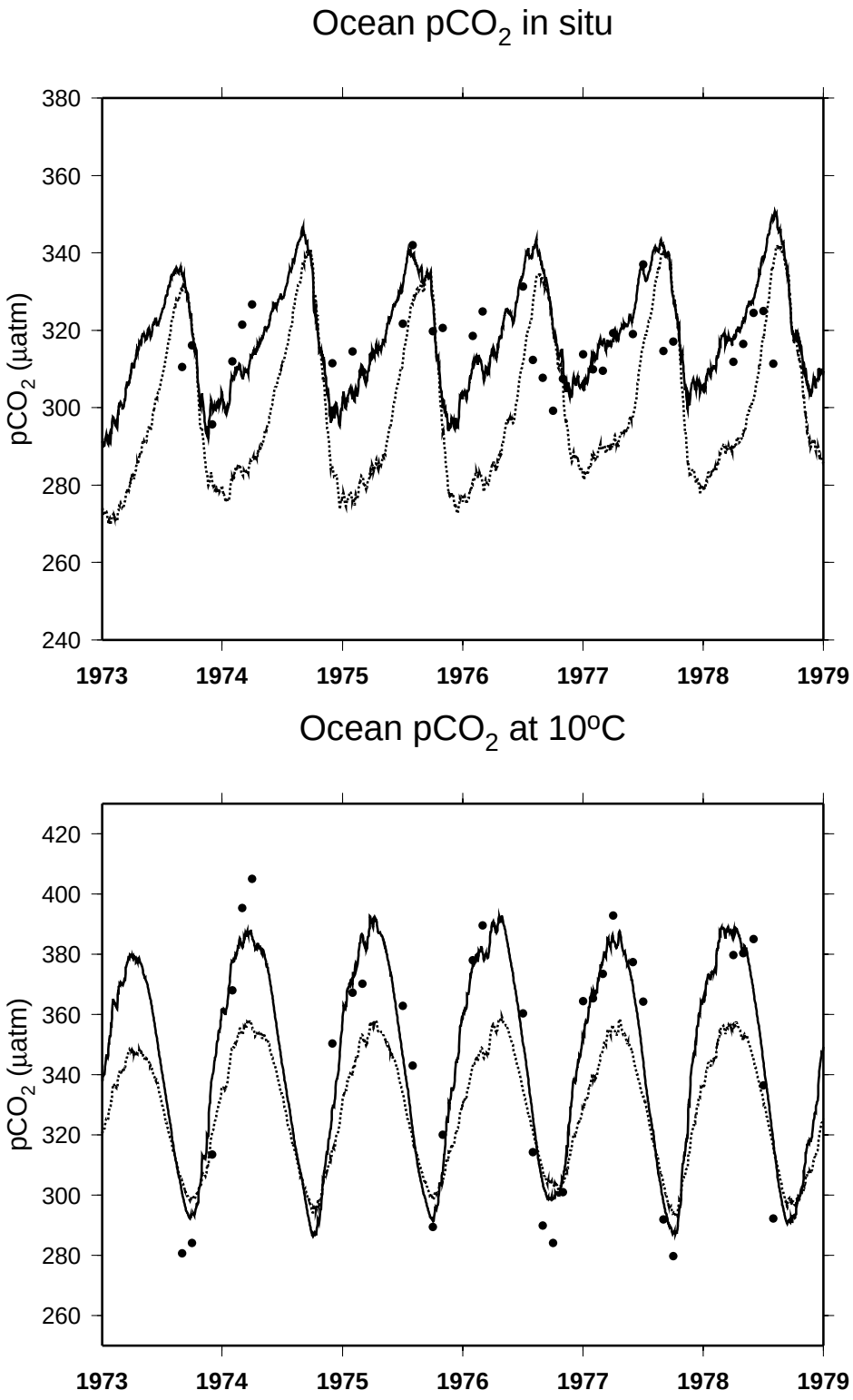

Figure 14. Comparison between model and observed *pCO$_2$* (in situ and normalized to 10 ºC) for the period of 1973-1978. Results from two model runs are shown: (1) the dotted line shows the model results using the gas exchange formulation of *Wanninkhof* [1992]; (2) the solid line shows the model results using the gas exchange formulation of *Wanninkhof and McGillis* [1999]. The solid black circles are the monthly averaged observed values.

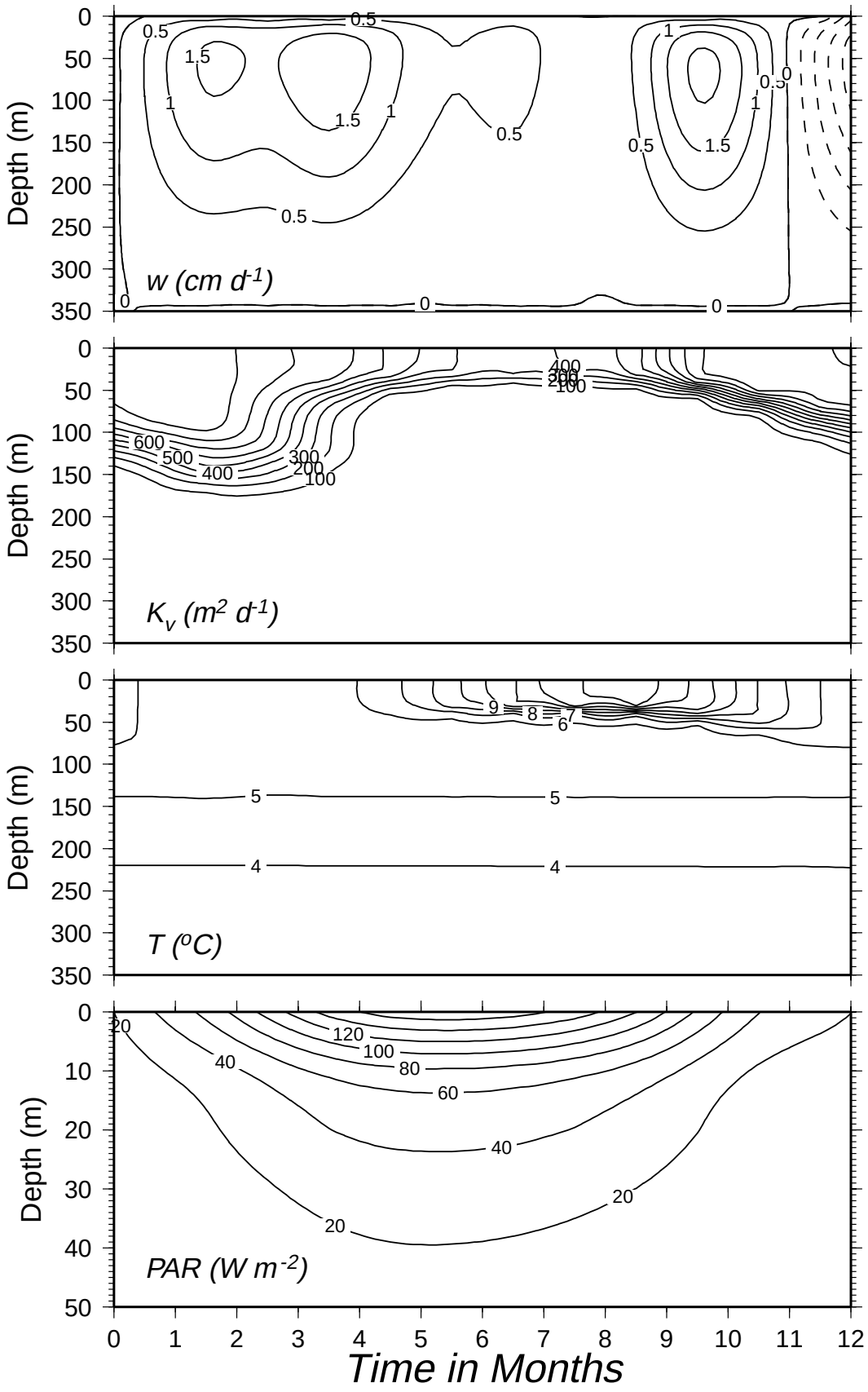

Figure 15. Seasonal variability of vertical velocity, vertical eddy diffusivity, temperature, and downwelling irradiance simulated by the model.

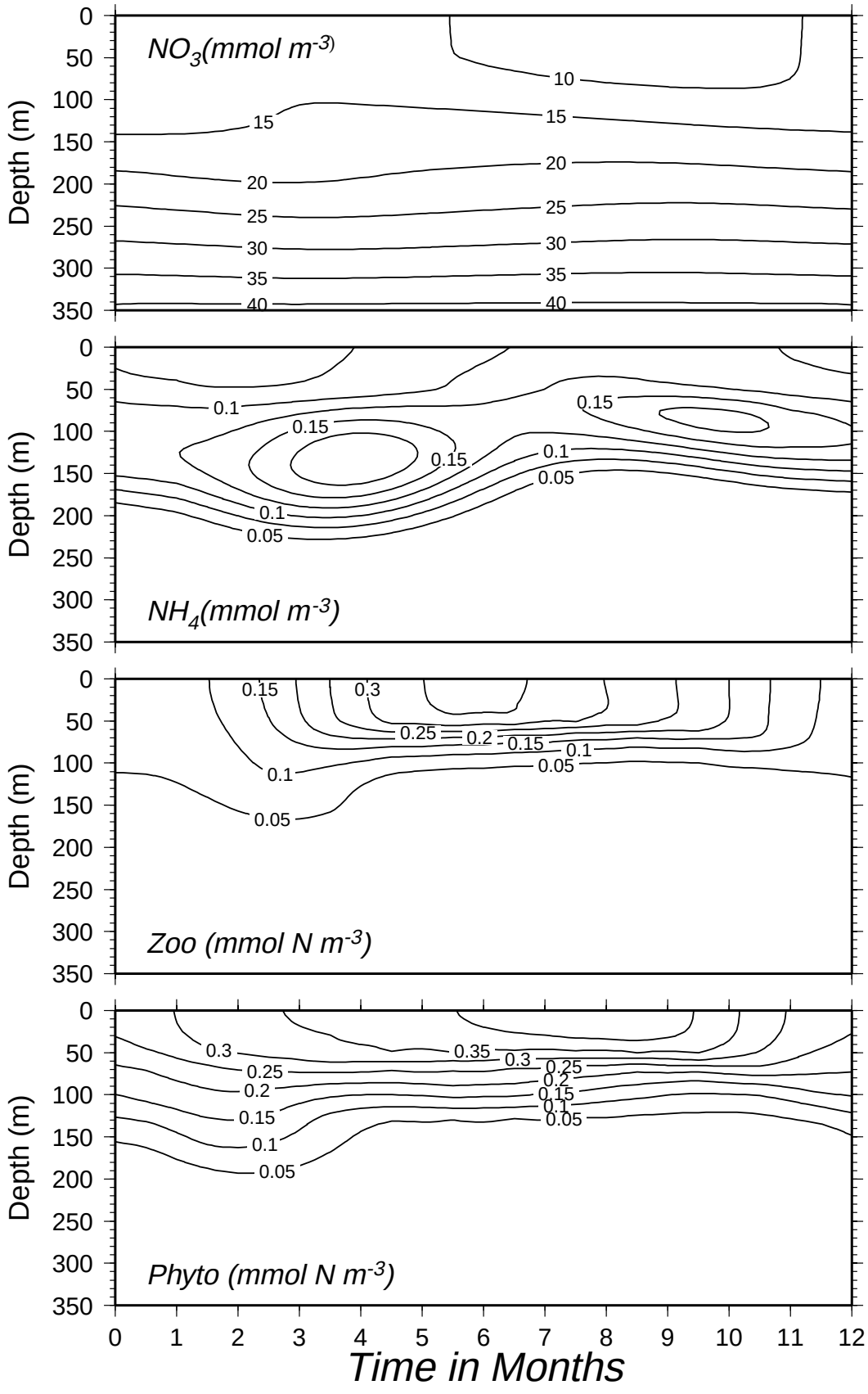

Figure 16. Seasonal variability of nitrate, ammonium, zooplankton, and phytoplankton concentrations simulated by the model.

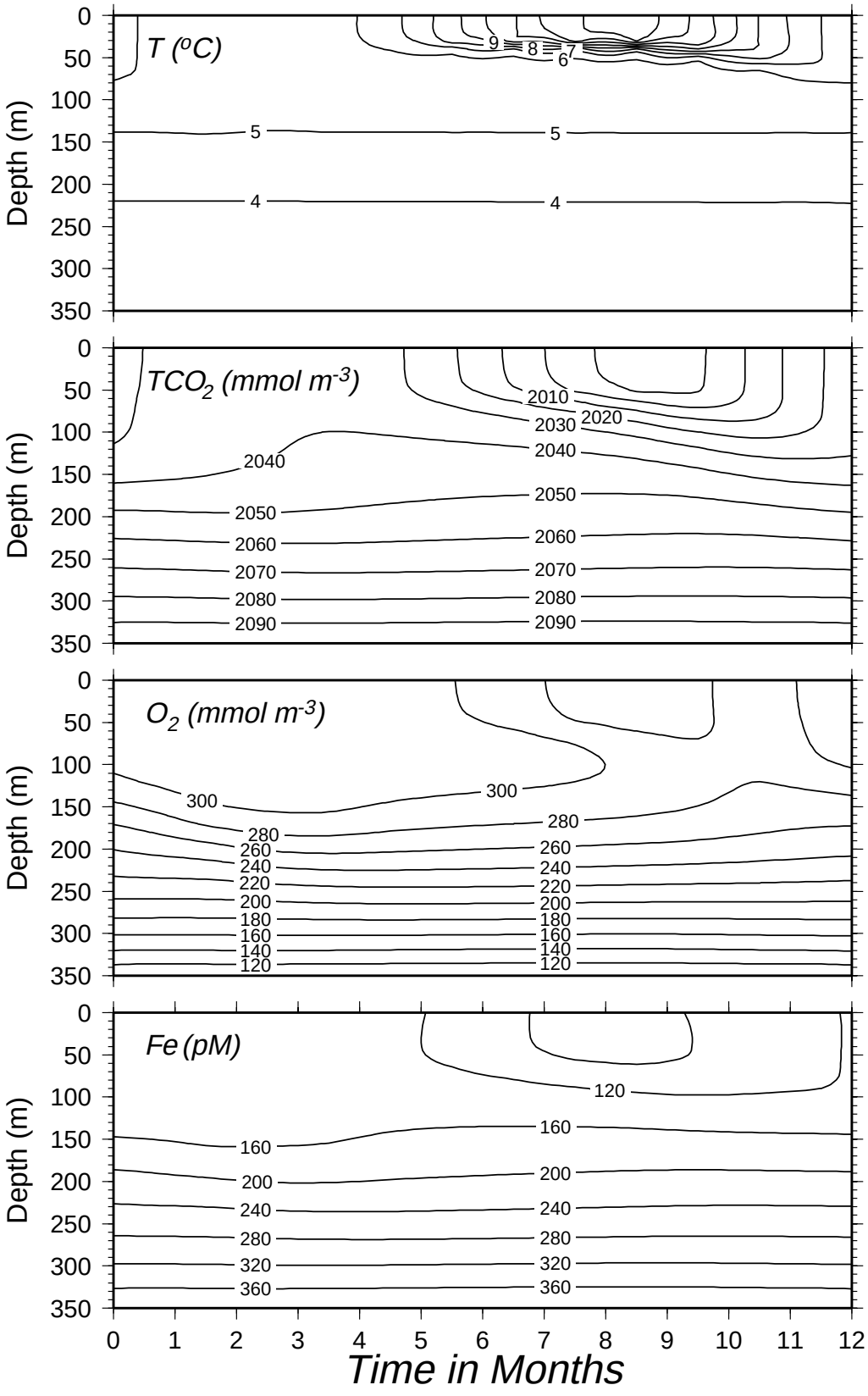

Figure 17. Seasonal variability of temperature, total carbon dioxide, oxygen, and iron concentrations simulated by the model.

6.0 INTERANNUAL VARIABILITY

The interannual variability of the major parameters simulated by the model is illustrated in the profile time series shown in Figures 19 and 20, and in the surface time series shown in Figure 21. The temperature profile shows distinct warm and cold periods. Two warm periods occur on the series, one during 1960-1965 and another during 1976-1980. The period during 1966-1975 exhibits colder (~1 °C) temperatures in the top 150 meters. The oxygen profile series shows higher (~20 mmol/kg) concentrations during the cold period due to increased solubility. The phytoplankton concentration in the upper 20 meters was higher (~0.1 mg/m^3) during the warmest temperature events (1961, 1963, and 1979).

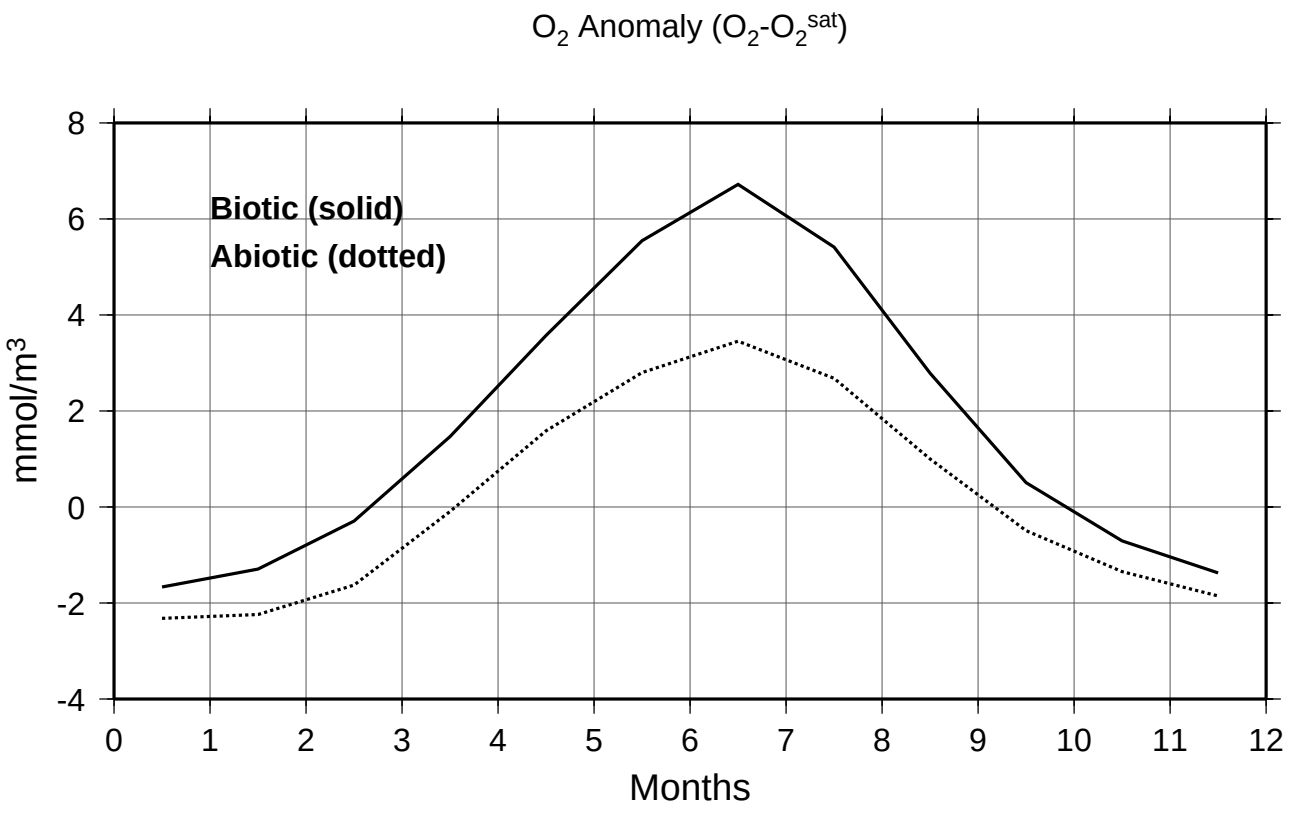

Figure 18. Seasonal variability of surface oxygen anomaly predicted by the model. Results from two runs are presented, an abiotic run (dotted line) and a biotic run (solid line).

The secular pCO_2 upward trend shown in the top tier of Figure 21 is manifested in the profile series of total carbon dioxide concentration in Figure 19. The carbon dioxide increase of about 20 mmol/m^3 in 20 years, caused by the increased surface flux, is noticeable at depths of up to 250 meters. The highest drawdown in the iron, nitrate, and carbon dioxide concentrations occurred during 1961-1963, a period of warmest euphotic zone temperatures during which solubility was lowest and phytoplankton growth was highest. Figure 22 shows the yearly and depth averaged (0-100 m) temperature and TCO_2 variability, and the surface CO_2 flux and oceanic pCO_2 variability for the period of 1960-1980. The interannual changes and trends are highlighted in this figure. Note the cooling trend in the temperature during the 1960s, followed by a warming trend during the mid to late 1970s. The air-sea CO_2 flux is always negative, indicating that OWS P is a sink of atmospheric CO_2. The pCO_2 trends upward almost monotonically showing an increase of about 30 µatm in 20 years. The TCO_2 follows the pCO_2 trend, showing that the atmosphere and ocean are tightly coupled at OWS P.

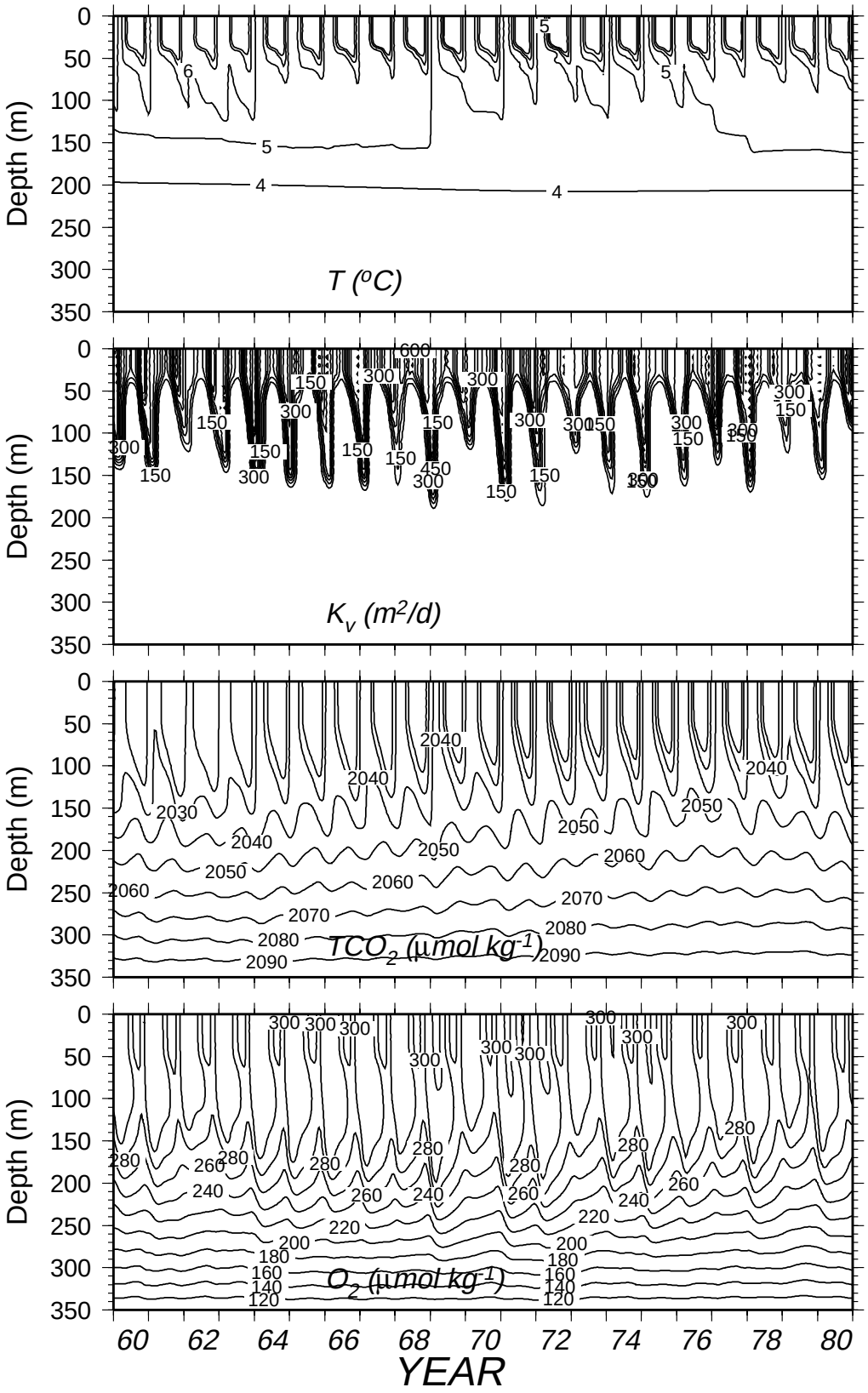

Figure 19. Interannual variability of temperature, vertical eddy diffusivity, total carbon dioxide, and oxygen simulated by the model.

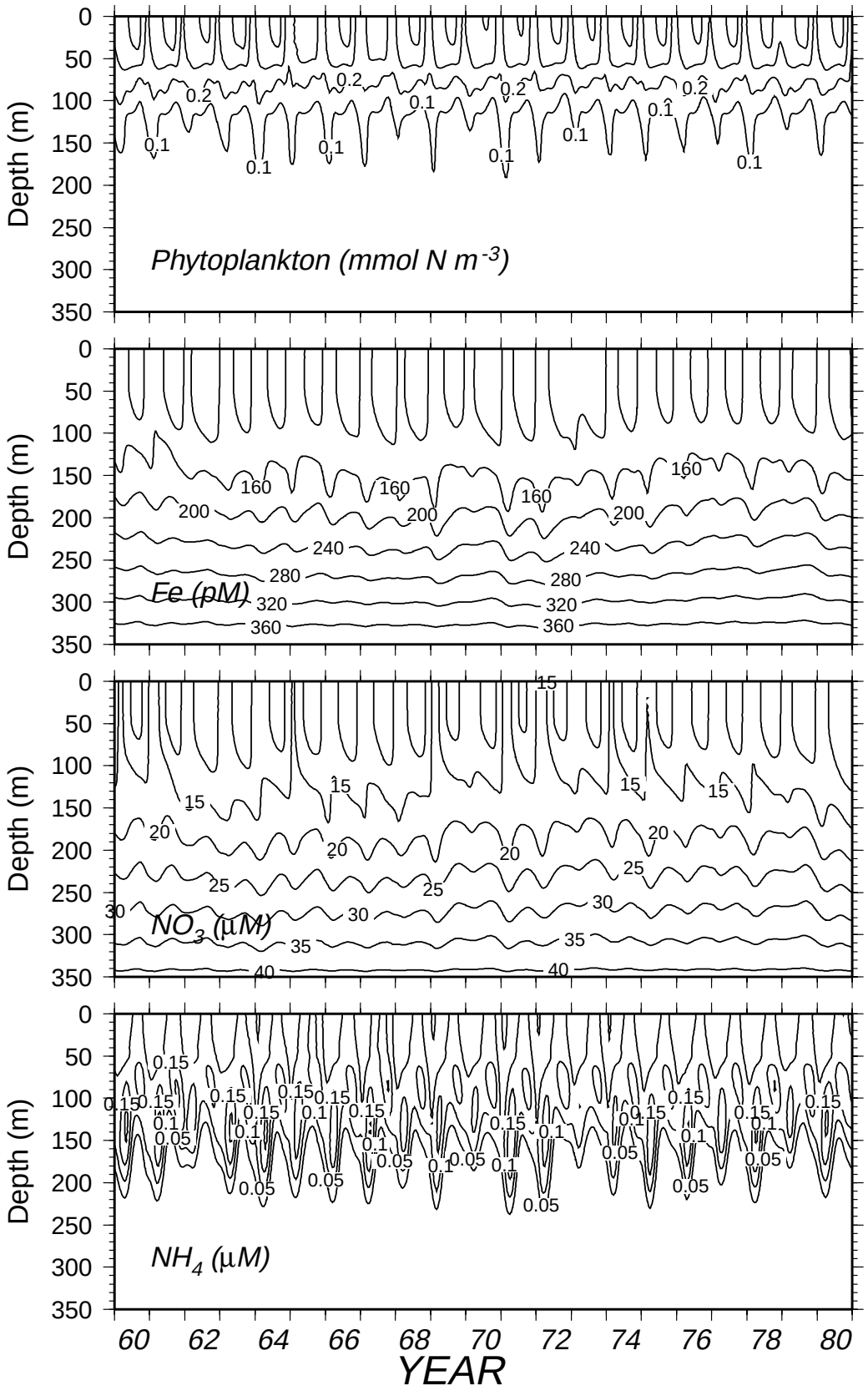

Figure 20. Interannual variability of phytoplankton, iron, nitrate, and ammonium simulated by the model.

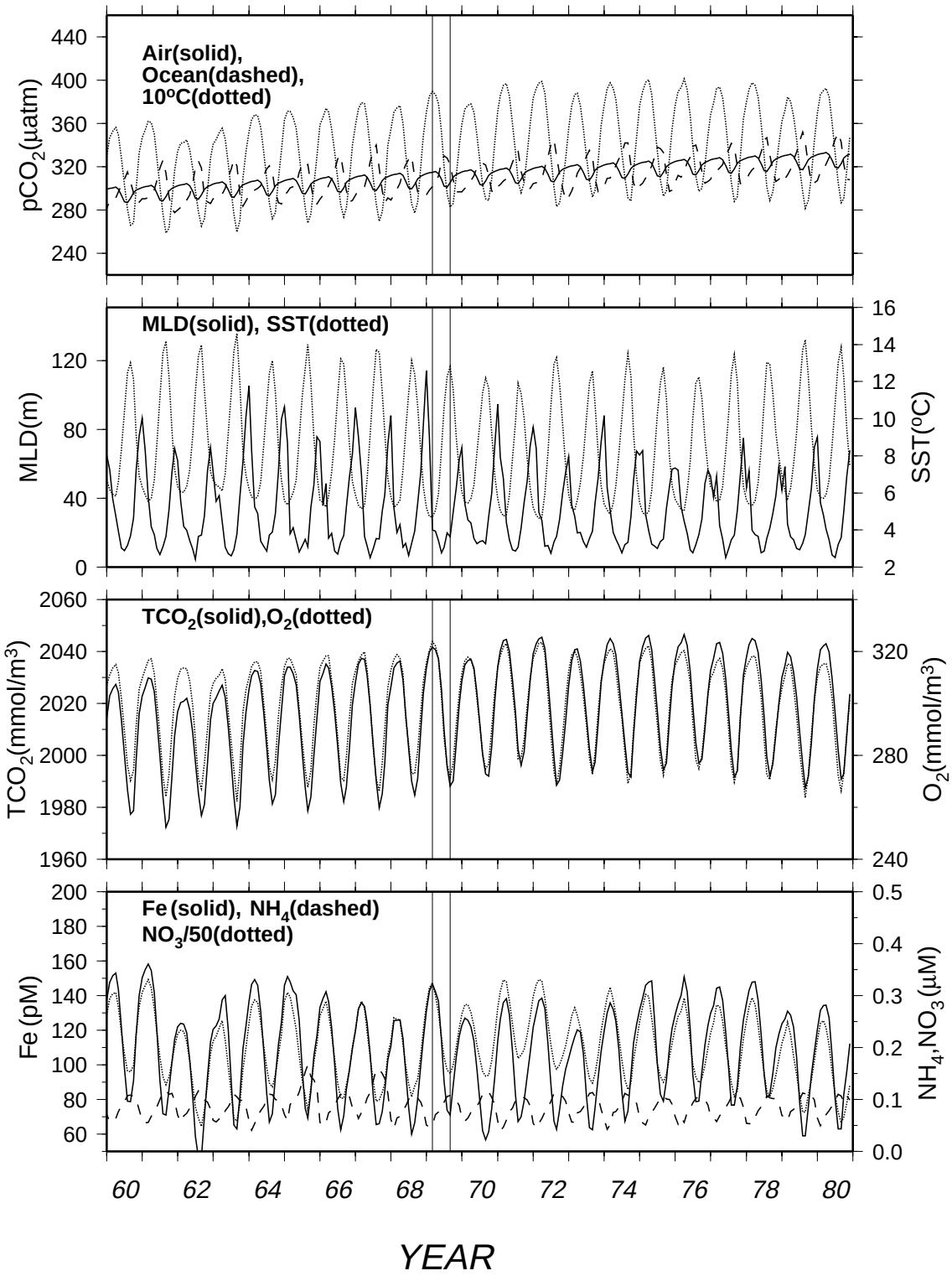

Figure 21. Time series of simulated atmospheric *pCO*$_2$, ocean *pCO*$_2$, SST, mixed layer depth, total carbon dioxide, oxygen, iron, nitrate, and ammonium.

7.0 CARBON FLUX BUDGET

Figure 23 represents the climatological (1960-1980) ecosystem carbon flux balance. The main compartments in this flow chart are the phytoplankton, zooplankton, respired DOC, and total CO_2 carbon stocks. The numbers indicate the carbon flux between ecosystem components in gC/m^2/yr. The ammonium and nitrate boxes were replaced by the net community production (76 gC/m^2/yr), which represents all sources and sinks of macronutrients combined (equation 14). Note that the air-sea (44 gC/m^2/yr) and bottom (23 gC/m^2/yr) carbon fluxes are balanced by the *POC+DOC* export (60 gC/m^2/yr) and fecal pellet loss (7 gC/m^2/yr) through the bottom. The total gross production (uptake) is 174 gC/m^2/yr. Therefore, the total carbon required for photosynthesis is partitioned among the following sources: 44% (76 gC/m^2/yr) originates from the TCO_2 pool - of these 44%, 5% comes from DOC respiration, 13% comes from the bottom flux, and 25% from the atmosphere (air-sea flux). The other 56% (98 gC/m^2/yr) of the required equivalent carbon comes from the recycling of zooplankton and phytoplankton losses (death, respiration, and fecal pellet production).

8.0 SUMMARY AND CONCLUSIONS

A coupled ecosystem/carbon flux model was developed, validated, and used to simulate biogeochemical parameters at OWS P. A series of sensitivity runs revealed that the most significant improvement in the simulation of the surface pCO_2 is obtained by the use of a recently developed cubic formulation for the gas exchange coefficient (*Wanninkhof and McGillis,* 1999). This result shows that the ocean and atmosphere are much more closely coupled at high (> 10 m/s) wind speeds than indicated by the previous wind-dependent formulations (*Liss and Merlivat,* 1986; *Tans et al*., 1990; *Wanninkhof,* 1992).

All biogeochemical parameters, when averaged over the period of available concurrent observations (1973-1978), are within less than 5% of the observed values. The only exception is the sea-air CO_2 flux which departs more significantly from previously reported values. We attribute this difference to the elusive nature of sea-air CO_2 estimates in the ocean and the variety of formulations used in the literature to derive the gas exchange coefficient. For example, our lowest CO_2 flux estimate is -29.6 gC/m^2/yr when we use the *Liss and Merlivat* [1986] gas exchange formulation. *Wong and Chan* [1991], also using the *Liss and Merlivat* [1986] gas exchange formulation, report a value of -8.4 g C/m^2/yr. Our CO_2 flux value is even higher (-45.6 gC/m^2/yr) when we use the *Wanninkhof and McGillis* [1999] gas exchange formulation. However, the model estimates for the surface flux and those derived from ΔpCO_2 measurements are not entirely equivalent because the model provides a dynamically coupled flux estimate, whereas the air-sea flux estimates from observed ΔpCO_2 are obtained from a relatively small number of discrete data points. Therefore, global estimates of air-sea CO_2 flux derived using air-sea flux models to extrapolate from observed pCO_2 may not be realistic. In the short term, fully prognostic models may give the best estimates provided that they achieve sufficient agreement with other observable quantities such as temperature, chlorophyll, and TCO_2.

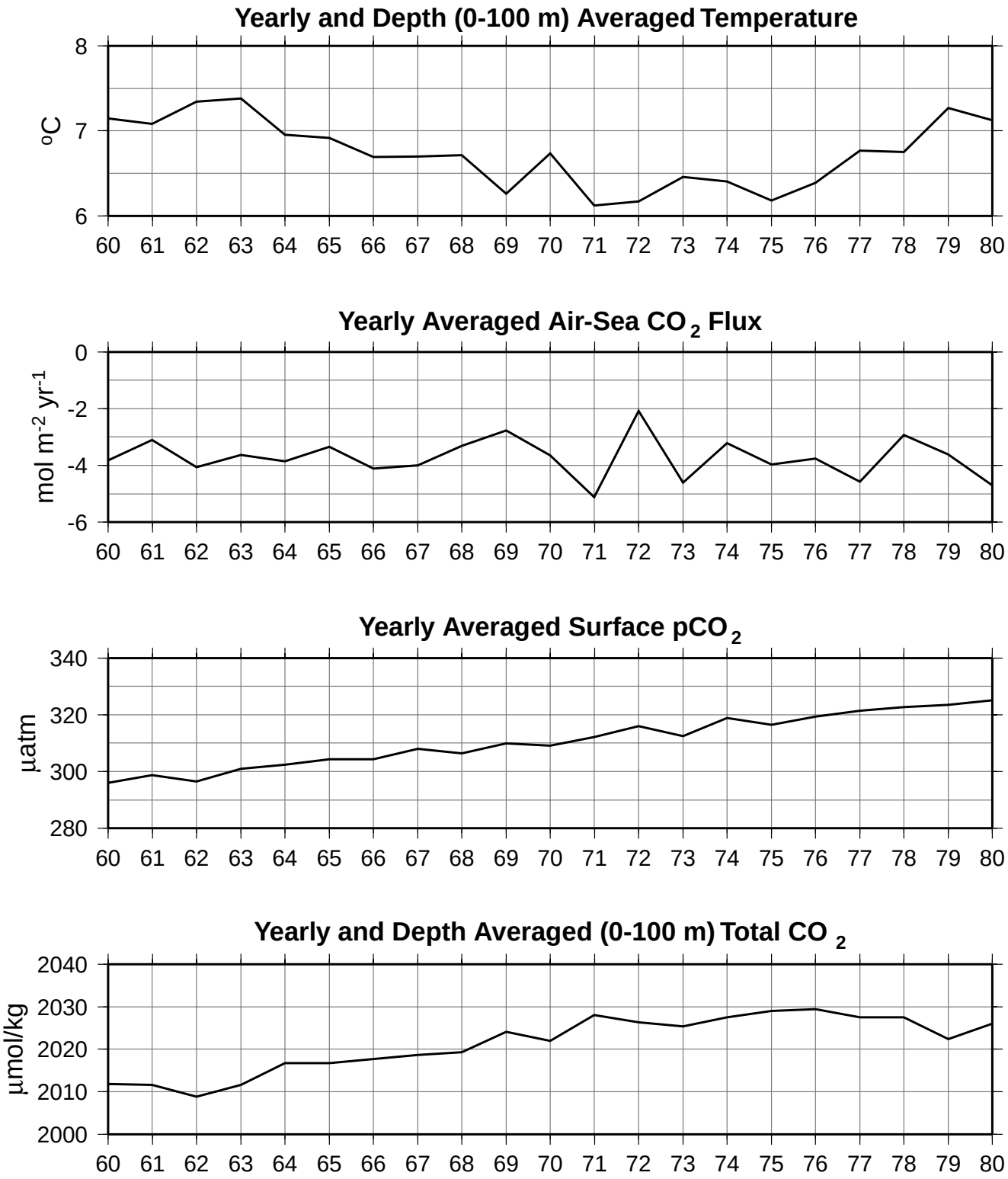

Figure 22. Yearly averaged time series of ocean temperature (0-100 m mean), air-sea carbon dioxide flux, surface carbon dioxide partial pressure, and total carbon dioxide concentration temperature (0-100 m mean) simulated by the model for the period of 1960-1980.

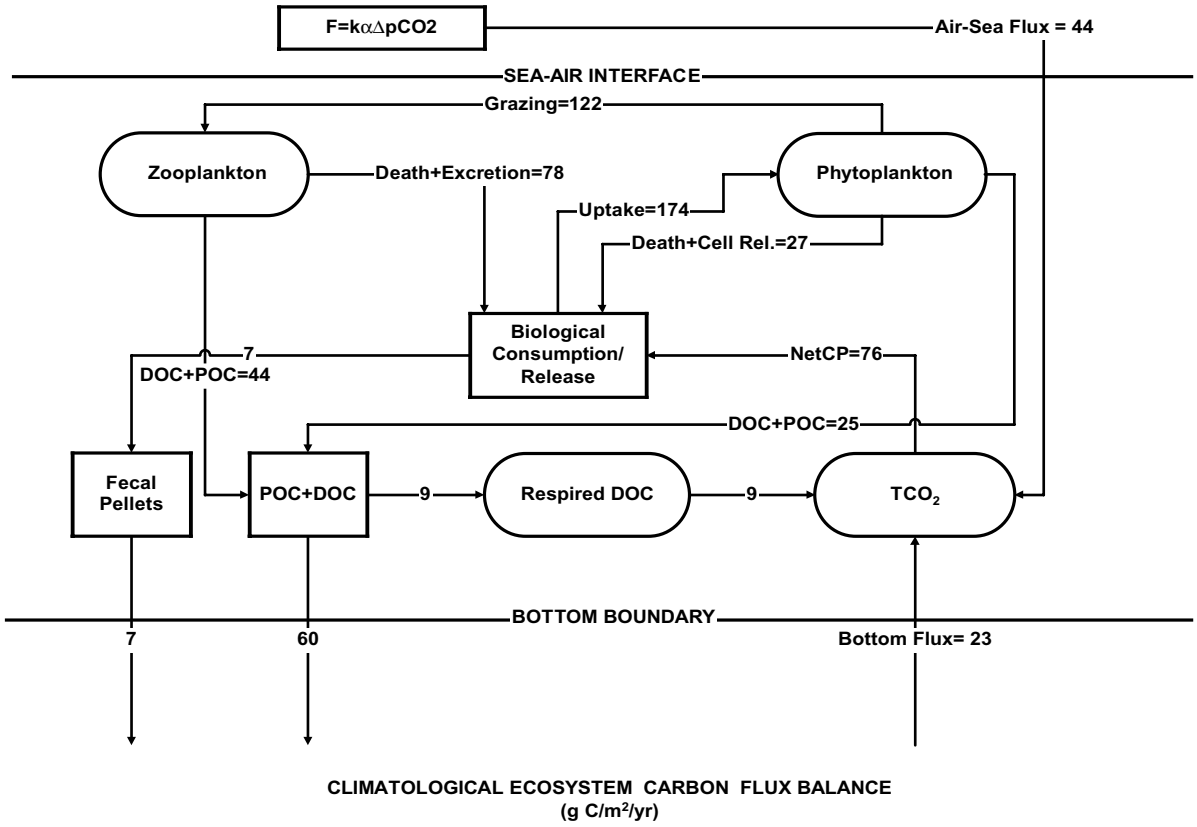

Figure 23. Flow chart of simulated climatological carbon flux balance showing the principal carbon exchange compartments in the coupled ecosystem/carbon-flux model.

REFERENCES

Andrié, C., C. Oudot, C. Genthon, and L. Merlivat, CO_2 fluxes in the tropical Atlantic during FOCAL cruises, *J. Geophys. Res., 91*, 11,741-11,755, 1986.

Antoine, D., and A. Morel, Modelling the seasonal course of the upper ocean pCO_2: (I). Development of a one-dimensional model, *Tellus, 47B*, 103-121, 1995.

Antoine, D., and A. Morel, Modelling the seasonal course of the upper ocean pCO_2:(II). Validation of the model and sensitivity studies, *Tellus, 47B*, 122-144, 1995.

Archer, D., S. Emerson, T. Powell, and C. S. Wong, Numerical hindcasting of sea surface pCO_2 at Weathership OWS P, *Prog. Oceanogr., 32*, 319-351, 1993.

Batrakov, G. F., A. A. Bezborodov, V. N. Yeremeyev, and A. D. Zemlyanoy, CO_2 exchange between Indian Ocean waters and the atmosphere, *Oceanology, 21*, 39-43, 1981.

Boyd, P. W., D. L. Muggli, D. E. Varela, R. H. Goldblatt, R. Chretien, K. J. Orians, and P. J. Harrison, In vitro iron enrichment experiments in the NE subarctic Pacific, *Mar. Ecology Progr. Ser., 136*, 179-193, 1996.

Broecker, W. S., and T.-H. Peng, The vertical distribution of radon in the BOMEX area, *Earth Planet. Sci. Lett., 11,* 99-108, 1971.

Broecker, W. S., and T.-H. Peng, Gas exchange rates between air and sea, *Tellus, 26*, 21-35, 1974.

Conkright, M., S. Levitus, and T. Boyer, *NOAA Atlas NESDIS 1, World Ocean Atlas 1994*, U. S. Dep. of Comm., Washington D. C., 1994.

Dobson, F. W., and S. D. Smith, Bulk models of solar radiation at sea, *Q. J. R. Meteorol. Soc., 114*, 165-182, 1988.

Duce, R. A., Sources, distributions, and fluxes of mineral aerosols and their relationship to climate, in *Aerosol Forcing of Climate*, R. J. Charlson and J. Heintzenberg, editors, John Wiley and Sons, 43-72, 1995.

Frost, B. W., A modelling study of processes regulating plankton standing stock and production in the open subarctic Pacific Ocean, *Prog. Oceanogr., 32*, 17-56, 1993.

Fushimi, K., Variation of carbon dioxide partial pressure in the western North Pacific surface water during the 1982-1983 El Niño event, *Tellus, Ser. B, 39*, 214-227, 1987.

Emerson, S., P. Quay, and P. A. Wheeler, Biological productivity determined from oxygen mass balance and incubation experiments, *Deep Sea Res.*, 40, 2351-2358, 1993.

Goyet, C., and A. Poisson, New determination of carbonic acid dissociation constants in sea water as a function of temperature and salinity, *Deep Sea Res., 36*, 1635-1654, 1989.

Gordon, L. I., P. K. Park, S. W. Hager, and T. R. Parsons, Carbon dioxide partial pressures in north Pacific surface waters - time variations, *J. Oceanogr. Soc. Japan, 27*, 81-90, 1971.

Gordon, L. I., P. K. Park, J. J. Kelley, and D. W. Hood, Carbon dioxide partial pressures in north Pacific surface waters, 2. General late summer distributions, *Mar. Chem., 1*, 191-198, 1973.

Inoue, H., Y. Sugimura, and K. Fushimi, *pCO2* and $\delta^{13}C$ in the air and surface sea water in the western North Pacific, *Tellus 39 B*, 228-242, 1987.

Inoue, H., and Y. Sugimura, Distributions and variations of oceanic carbon dioxide in the western North Pacific, eastern Indian, Southern Ocean south of Australia, Tellus 40 B, 308-320, 1988.

Keeling, C. D., Carbon dioxide in surface ocean waters, 4, Global distribution, *J. Geophys. Res., 73*, 4543-4554, 1968.

Liss, P. S., Tracers of air-sea gas exchange, *Phil. Trans. R. Soc. Lond., A 325*, 93-103, 1988.

Liss, P. S., and L. Merlivat, Air-sea exchange rates: Introduction and synthesis. In: *The Role of Air-Sea Exchange in Geochemical Cycling*, P. Buat-Ménard, editor, NATO ASI Series C: Mathematical and Physical Sciences, Vol. 185, pp. 113-128, 1986.

Maldonado, M. T., P. W. Boyd, P. J. Harrison, and N. M. Price, Co-limitation of phytoplankton growth by light and Fe during winter in the NE subarctic Pacific Ocean, *Deep-Sea Res. II*, 46, 2475-2485, 1999.

Martin, J. H., S. E. Fitzwater, W. W. Broenkow, VERTEX: phytoplankton/iron studies in the Gulf of Alaska, *Deep-Sea Res., 36*, 645-680, 1989.

McClain, C. R., K. Arrigo, K.-S. Tai, and D. Turk, Observations and simulations of physical and biological processes at ocean weather Station P, 1951-1980, *J. Geophys. Res., 101*, 3697-3713, 1996.

McClain, C. R., S. R. Signorini, K.-S. Tai, K. Arrigo, and R. Murtugudde, An ecosystem model for the simulation of physical and biological oceanic processes - IDAPAK User's guide and applications, NASA/TM-1998-206856, NASA Goddard Space Flight Center, Greenbelt, Maryland, April 1998.

Millero, F. J., K. Lee, and M. Roache, Distribution of alkalinity in the surface waters of the major oceans, *Mar. Chem., 60*, 111-130, 1998.

Murphy, P. P., D. E. Harrison, R. A. Feely, T. Takahashi, R. F. Weiss, and R. H. Gammon, Variability of ΔpCO_2 in the subarctic North Pacific. A comparison of results from four expeditions, *Tellus, 50B*, 185-204, 1998.

Oudot, C., and C. Andrié, Variabilité des pressions partielles de CO_2 océanique et atmosphérique dans l'Atlantique tropical, *Oceanol. Acta 9*, 169-177, 1986.

Oudot, C., and C. Andrié, Short-term changes in the partial pressure of CO_2 in eastern tropical Atlantic surface seawater and in atmospheric CO_2 mole fraction, *Tellus 41 B*, 537-553, 1989.

Oudot, C., and C. Andrié, and Y. Montel, Evolution du CO_2 océanique et atmosphérique sur la période 1982-1984 dans l'Atlantique tropical, *Deep-Sea Res., 34*, 1107-1137, 1987.

Peng, T.-H., T. Takahashi, and W. S. Broecker, Surface radon measurements in the North Pacific Ocean OWS P, *J. Geophys. Res., 79*, 1772-1780, 1974.

Peng, T.-H., W. S. Broecker, G. C. Mathiew, and Y.-H. Li, Radon evasion rates in the Atlantic and Pacific Oceans as determined during the Geosecs program, *J. Geophys. Res., 84*, 2471-2486, 1979.

Pond, S., and G. L. Pickard, *Introductory Dynamic Oceanography*, 241 pp., Pergamon, Tarrytown, N. Y., 1978.

Smethie, W. M., Jr., T. Takahashi, D. W. Chipman, and J. R. Ledwell, Gas exchange flux in tropical Atlantic Ocean determined from ^{222}Rn and pCO_2, *J. Geophys. Res., 90*, 7005-7022, 1985.

Sundquist, E. T., Geological perspectives on carbon dioxide and carbon cycle, in *The Carbon Cycle and Atmospheric CO_2: Natural Variations Archean to present, Geophys. Monogr. Ser.*, vol. 32, edited by E. T. Sundquist and W. S. Broecker, pp 5-59, AGU, Washington, D. C., 1985.

Takahashi, T., D. Chipman, and T. Volk, Geographical, seasonal, and secular variations of the partial pressure of CO_2 in surface waters of the North Atlantic TTO program, in *Carbon Dioxide, Science and Consensus* (CONF-820970), Institute for Energy Analysis, Oak Ridge Associated Universities, Washington, D. C., 123-145, 1983.

Takahashi, T., J. Olafsson, J. G. Goddard, D. W. Chipman, and S. C. Sutherland, Seasonal variations of CO_2 and nutrients in the high-latitude surface oceans: A comparative study, *Global Biogeochem. Cycles, 7*, 843-878, 1993.

Takahashi, T., R. A. Feely, R. F. Weiss, R. H. Wanninkhof, D. W. Chipman, S. C. Sutherland, and T. T. Takahashi, Global air-sea flux of CO_2: An estimate based on measurements of sea-air pCO_2 difference, *Proc. Natl. Acad. Sci.*, vol. 94, pp. 8292-8299, 1997.

Taylor, A. H., A. J. Watson, M. Ainsworth, J. E. Robertson, and D. R. Turner, A modeling investigation of the role of phytoplankton in the balance of carbon at the surface of the North Atlantic, *Global Biogeochem. Cycles, 5*, 151-171, 1991.

Tegen, I., and I. Fung, Modeling of mineral dust in the atmosphere: Sources, transport, and optical thickness, *J. Geophys. Res.*, 99, 22,897-22,914, 1994.

Weiss, R. F., The solubility of nitrogen, oxygen and argon in water and seawater, *Deep Sea Res., 17*, 721-735, 1970.

Weiss, R. F., Carbon dioxide in water and seawater: The solubility of a non-ideal gas, *Mar. Chem., 2*, 203-215, 1974.

Wanninkhof, R., and W. R. McGillis, A cubic relationship between air-sea exchange and wind speed, *Geophys. Res. Lett., 26*, 1889-1892, 1999.

Wanninkhof, R., Relationship between wind speed and gas exchange over the ocean, *J. Geophys. Res., 97*, 7373-7382, 1992.

Wong, C. S., and Y.-H. Chan, Temporal variations in the partial pressure and flux of CO_2 at ocean Station P in the subarctic northeast Pacific Ocean, *Tellus, 43B*, 206-223, 1991.

REPORT DOCUMENTATION PAGE

Form Approved
OMB No. 0704-0188

1. AGENCY USE ONLY *(Leave blank)*

2. REPORT DATE
June 2000

3. REPORT TYPE AND DATES COVERED
Technical Publication

4. TITLE AND SUBTITLE
One-Dimensional Coupled Ecosystem-Carbon Flux Model for the Simulation of Biogeochemical Parameters at Ocean Weather Station P

5. FUNDING NUMBERS
970.2

6. AUTHOR(S)
S. Signorini, C. McClain, J. Christian, C.S. Wong

7. PERFORMING ORGANIZATION NAME(S) AND ADDRESS (ES)
Goddard Space Flight Center
Greenbelt, Maryland 20771

8. PEFORMING ORGANIZATION REPORT NUMBER
2000-01898-0

9. SPONSORING / MONITORING AGENCY NAME(S) AND ADDRESS (ES)
National Aeronautics and Space Administration
Washington, DC 20546-0001

10. SPONSORING / MONITORING AGENCY REPORT NUMBER
TP—2000–209892

11. SUPPLEMENTARY NOTES
S. Signorini; SAIC General Sciences Corporation; Beltsville, Maryland
J. Christian; Universities Space Research Assoc.; NASA/GSFC; Greenbelt, Maryland
C.S. Wong; Centre for Ocean Climatic Chemistry; Institute of Ocean Studies; Sidney, British Columbia

12a. DISTRIBUTION / AVAILABILITY STATEMENT
Unclassified–Unlimited
Subject Category: 42
Report available from the NASA Center for AeroSpace Information,
7121 Standard Drive, Hanover, MD 21076-1320. (301) 621-0390.

12b. DISTRIBUTION CODE

13. ABSTRACT *(Maximum 200 words)*

In this Technical Publication, we describe the model functionality and analyze its application to the seasonal and interannual variations of phytoplankton, nutrients, pCO_2 and CO_2 concentrations in the eastern subarctic Pacific at Ocean Weather Station P (OWSP, 50 °N 145 °W). We use a verified one-dimensional ecosystem model (*McClain et al*., 1996), coupled with newly incorporated carbon flux and carbon chemistry components, to simulate 22 years (1958-1980) of pCO_2 and CO_2 variability at Ocean Weather Station P (OWS P). This relatively long period of simulation verifies and extends the findings of previous studies (*Wong and Chan*, 1991; *Archer et al*., 1993; *Antoine and Morel*, 1995a; *Antoine and Morel*, 1995b) using an explicit approach for the biological component and realistic coupling with the carbon flux dynamics. The slow currents and the horizontally homogeneous ocean in the subarctic Pacific make OWS P one of the best available candidates for modeling the chemistry of the upper ocean in one dimension. The chlorophyll and ocean currents composite for 1998 shown in Figure 1 illustrates this premise. The chlorophyll concentration map was derived from SeaWiFS data and the currents are from an OGCM simulation (from *R. Murtugudde*).

14. SUBJECT TERMS
ecosystem dynamics, biogeochemistry, carbon flux

15. NUMBER OF PAGES
36

16. PRICE CODE

17. SECURITY CLASSIFICATION OF REPORT	18. SECURITY CLASSIFICATION OF THIS PAGE	19. SECURITY CLASSIFICATION OF ABSTRACT	20. LIMITATION OF ABSTRACT
Unclassified	Unclassified	Unclassified	UL